

Fully gapped s -wave superconductivity enhanced by magnetic criticality in heavy-fermion systems

Rina Tazai and Hiroshi Kontani

Department of Physics, Nagoya University, Furo-cho, Nagoya 464-8602, Japan

(Received 30 July 2018; revised manuscript received 2 October 2018; published 5 November 2018)

In heavy-fermion systems, higher-rank multipole operators are active thanks to the strong spin-orbit interaction (SOI), and the role of diverse multipole fluctuations on the pairing mechanism attracts a lot of attention. Here, we study a mechanism of superconductivity in heavy-fermion systems, by focusing on the impact of vertex corrections (VCs) for the pairing interaction going beyond the Migdal approximation. In heavy-fermion systems, strong interference between multipole fluctuations cause significant VCs that represent many-body effects beyond mean-field-type approximations. Especially, the coupling constants between electrons and charged bosons, including the electron-phonon coupling constant, are strongly magnified by the VCs. For this reason, moderate even-rank (=electric) multipole fluctuations give large attractive interaction, and therefore s -wave superconductivity can emerge in heavy-fermion systems. In particular, phonon-mediated superconductivity is expected to be realized near the magnetic criticality, thanks to the VCs due to magnetic multipole fluctuations. The present mechanism may be responsible for the fully gapped s -wave superconducting state realized in CeCu_2Si_2 .

DOI: [10.1103/PhysRevB.98.205107](https://doi.org/10.1103/PhysRevB.98.205107)**I. INTRODUCTION**

Heavy-fermion systems are very interesting platform of exotic electronic states induced by strong Coulomb interaction and spin-orbit interaction (SOI) on f electrons. In Ce-based compounds, $4f^1$ configuration is realized in Ce^{3+} ion. Due to strong SOI, the total angular momentum $J = L + S$ becomes good quantum number. Since the energy of $J = 5/2$ multiplet is about 0.3 eV lower than that of $J = 7/2$ multiplet, the latter can be safely dropped in the theoretical model. In tetragonal crystals, the degeneracy of $J = 5/2$ multiplet is separated into three Kramers doubles due to the crystalline electric field (CEF). Usually, the CEF splitting energy is of order 1 meV–10 meV.

In many f -electron systems, magnetic fluctuations cause interesting quantum critical phenomena and unconventional superconductivity [1–7]. In addition, higher-rank multipole operators are also active thanks to the strong SOI of f electrons. For this reason, various interesting multipole order and fluctuations are caused by strong f -electron interaction. As an example of higher-rank order, CeB_6 exhibits quadrupole (rank 2) order and field-induced octupole (rank 3) order [8,9]. Also, emergence of hexadecapole (rank 4) in $\text{PrRu}_4\text{P}_{12}$ [10] and hexadecapole or dotriacontapole (rank 5) in URu_2Si_2 [11–13] have been discussed. The fluctuations of these multipole operators mediate interesting unconventional superconductivity. For example, d -wave superconductivity appears next to the magnetic order phase in CeMIn_5 ($M = \text{Rh}, \text{Co}, \text{Ir}$) [14]. In addition, superconductivity appears next to the quadrupole order in $\text{PrT}_2\text{Zn}_{20}$ ($T = \text{Rh}$ and Ir) [15] and $\text{PrT}_2\text{Al}_{20}$ ($T = \text{V}, \text{Ti}$) [16]. These Pr-based superconductors indicate that the higher-rank (≥ 2) multipole fluctuations inherent in f -electron systems mediate exotic superconducting states.

CeCu_2Si_2 is the first discovered heavy-fermion superconductor [17,18], and its discovery triggered huge amount of research on unconventional superconductivity in various

compounds [19]. At ambient pressure, CeCu_2Si_2 shows superconducting transition at $T_c \approx 0.6$ K near the magnetic instability [20]. Under pressure, T_c suddenly increases to 1.5 K at $P_c \approx 4.5$ GPa. For long time, CeCu_2Si_2 has been considered as a typical d -wave superconductor mediated by magnetic fluctuations. However, d -wave nodal gap structure contradicts with exponentially small specific heat at $T \ll T_c$ as reported in Refs. [21,22]. Later, the fully gapped state is confirmed by the measurements of thermal conductivity and penetration depth at very low temperatures [23,24]. In addition, the robustness of T_c against randomness indicates that plain s -wave superconductivity without sign-reversal is realized in CeCu_2Si_2 [23].

It is a significant challenge for theorists to establish a realistic microscopic theory of fully gapped s -wave superconductivity in heavy-fermion systems, against large Coulomb repulsion. It is believed that fluctuations of even-rank multipole operators, such as charge, quadrupole and hexadecapole operators, mediate attractive pairing interaction. To realize large even-rank multipole fluctuations, at least two Kramers doublets should contribute to the Fermi surface, if the charge (rank 0) fluctuations are suppressed by Coulomb interaction. In fact, in CeCu_2Si_2 at ambient pressure, two Kramers doublets form the Kondo resonance below 10 K according to the first-principles study based on the LDA+DMFT [25]. Pressure-induced change in multiorbital nature may be a key to understand the P - T phase diagram in CeCu_2Si_2 [25–27].

In the random-phase-approximation (RPA), even-rank multipole fluctuations are always smaller than odd-rank ones. Therefore the obtained gap structure inevitably possesses sign reversal within the Migdal approximation [28]. This discrepancy indicates the significance of higher-order many-body effects called the vertex corrections (VCs). In fact, the VC for the electron-boson coupling, which we call U -VC, has been studied in Refs. [2,3,5,29–33]. The violation of

Migdal theorem [34] due to the Maki-Thompson (MT) and Aslamazov-Larkin (AL) VCs, which are respectively the first-order and second-order corrections with respect to the susceptibility, have been studied in Refs. [5,29,33,35]. In multi-orbital systems, moderate orbital fluctuations induce strong attractive pairing interaction thanks to the AL-type U -VC [35,36]. However, strong SOI in f -electron systems has prevented the detailed analysis of the VCs. Thus it is highly required to construct the theoretical formalism to analyze the VCs in systems with strong SOI. We stress that the DMFT has been successfully applied to f -electron systems [11,25,37–41], while strong k -dependence of VCs near the magnetic quantum-critical-point (QCP) is not fully taken into consideration.

In this paper, we propose a mechanism of s -wave superconductivity in multi-orbital heavy-fermion systems by focusing on the VCs beyond Migdal approximation. Near the magnetic QCP, various types of multipole fluctuations develop simultaneously, due to the combination of strong SOI and Coulomb interaction. The developed multipole fluctuations give significant VCs in heavy-fermion systems. Especially, the VCs significantly magnify the attractive pairing interaction due to even-rank multipole fluctuations, so the Migdal theorem is no more valid. Due to this mechanism, s -wave superconductivity can be realized in heavy-fermion systems, once moderate (phonon-induced) quadrupole or hexadecapole fluctuations exist. The s -wave superconductivity is strongly enhanced near the magnetic criticality. The present mechanism may be responsible for the fully gapped superconducting state realized in CeCu_2Si_2 .

In $3d$ -electron systems, the AL-type VCs are efficiently calculated by using the $\text{SU}(2)$ symmetry in the spin space. Thus the same formalism cannot be applied to $5d$ or f -electron systems because of the violation of $\text{SU}(2)$ symmetry. To overcome this difficulty, we introduce a natural two-orbital periodic Anderson model, in which the pseudospin of f electron satisfies the axial rotational symmetry. By virtue of this fact, we can analyze complicated VCs efficiently. In the present model, 16 type multiple operators (rank 0–5) are active, so we can discuss rich physics associated with higher-rank multipole operators.

II. MODEL

In this section, we derive an useful two-orbital periodic Anderson model (PAM) for CeCu_2Si_2 , in which we can define the pseudospin that satisfy the conservation law. For this purpose, we first introduce a general three-orbital $J = 5/2$ PAM for describing $4f^1$ electrons in Ce-based compounds. The kinetic term is given by

$$\hat{H}_0^{\text{general}} = \sum_{k\sigma} \epsilon_k c_{k\sigma}^\dagger c_{k\sigma} + \sum_{kl\Sigma} E_l f_{kl\Sigma}^\dagger f_{kl\Sigma} + \sum_{kl\sigma\Sigma} (V_{kl\sigma\Sigma}^* f_{kl\Sigma}^\dagger c_{k\sigma} + V_{kl\sigma\Sigma} c_{k\sigma}^\dagger f_{kl\Sigma}), \quad (1)$$

where $c_{k\sigma}^\dagger$ ($c_{k\sigma}$) is a creation (annihilation) operator for s electron with momentum \mathbf{k} , spin σ , and energy ϵ_k . $f_{kl\Sigma}^\dagger$ ($f_{kl\Sigma}$) is a creation (annihilation) operator for f electron with \mathbf{k} ,

orbital l ($l = 1, 2, 3$), pseudospin Σ , and energy E_l . $V_{kl\sigma\Sigma}$ is the hybridization term between f and s electrons.

Here, we derive an useful simplified PAM for CeCu_2Si_2 from Eq. (1). According to the LDA+DMFT study for CeCu_2Si_2 [25], the following two Kramers doublets give dominant DoS around the Fermi energy at ambient pressure. They are expressed in the J_z basis as

$$\begin{aligned} |f_1 \uparrow\rangle &= a |-\frac{5}{2}\rangle + b |+\frac{3}{2}\rangle, \\ |f_1 \downarrow\rangle &= a |+\frac{5}{2}\rangle + b |-\frac{3}{2}\rangle, \\ |f_2 \uparrow\rangle &= -a |+\frac{3}{2}\rangle + b |-\frac{5}{2}\rangle, \\ |f_2 \downarrow\rangle &= -a |-\frac{3}{2}\rangle + b |+\frac{5}{2}\rangle, \end{aligned} \quad (2)$$

where \uparrow (\downarrow) denotes pseudospin up (down) of f_l -electron ($l = 1, 2$). We drop the third Kramers doublet $|f_3\rangle = |J_z = \pm\frac{1}{2}\rangle$, since it gives negligibly small weight near the Fermi level. We study 2D square lattice model as shown in Fig. 1(a). Both f and s orbitals are on Ce ion. For simplicity, we consider only the above-mentioned two orbitals. We introduce only the nearest neighbor s - f and s - s hopping integrals. In this case, f electron with pseudospin \uparrow (\downarrow) hybridizes with only s electron with \uparrow (\downarrow) as we confirm in Appendix A. Thus the pseudospin is conserved, and we can put $\Sigma = \sigma$. In the present two-orbital model, the kinetic term is given by

$$\begin{aligned} \hat{H}_0 &= \sum_{k\sigma} \epsilon_k c_{k\sigma}^\dagger c_{k\sigma} + \sum_{kl\sigma} E_l f_{kl\sigma}^\dagger f_{kl\sigma} \\ &+ \sum_{kl\sigma} (V_{kl\sigma}^* f_{kl\sigma}^\dagger c_{k\sigma} + V_{kl\sigma} c_{k\sigma}^\dagger f_{kl\sigma}) \\ &= \sum_{k\sigma} \hat{a}_{k\sigma}^\dagger \hat{h}_k^\sigma \hat{a}_{k\sigma}, \end{aligned} \quad (3)$$

where σ is the real (pseudo) spin for s (f) electron and $\hat{a}_{k\sigma}^\dagger \equiv (f_{k1\sigma}^\dagger, f_{k2\sigma}^\dagger, c_{k\sigma}^\dagger)$. By using the Slater-Koster tight-binding method [42,43], the s - f hybridizations are given as

$$\begin{aligned} V_{k f_1 \uparrow} &= -\sqrt{\frac{3}{14}} t_{sf} (a\sqrt{5} + b) (\sin k_y - i \sin k_x), \\ V_{k f_1 \downarrow} &= \sqrt{\frac{3}{14}} t_{sf} (a\sqrt{5} + b) (\sin k_y + i \sin k_x), \\ V_{k f_2 \uparrow} &= \sqrt{\frac{3}{14}} t_{sf} (a - \sqrt{5}b) (\sin k_y - i \sin k_x), \\ V_{k f_2 \downarrow} &= -\sqrt{\frac{3}{14}} t_{sf} (a - \sqrt{5}b) (\sin k_y + i \sin k_x). \end{aligned} \quad (4)$$

Hereafter, we simply put $a = 1$, $b (= \sqrt{1 - a^2}) = 0$. Actually, the relation $a \simeq 1$ is reported by recent resonant x-ray scattering experiment in Ref. [44]. In this case, we obtain $|V_{k f_1 \sigma} / V_{k f_2 \sigma}| = \sqrt{5}$. Thus f_1 orbital is more itinerant than f_2 orbital. This feature is consistent with the results of previous DMFT calculation for CeCu_2Si_2 in Ref. [25], which shows $V_{k f_2 \sigma} \approx 2V_{k f_1 \sigma}$. The schematic picture of the s - s and s - f hopping integrals are shown in Fig. 1(a). We fix the parameters $\epsilon_k = 2t_{ss}(\cos k_x + \cos k_y) + \epsilon_0$, $t_{ss} = -1.0$, $\epsilon_0 = 3.0$, $t_{sf} = 0.7$, and f -electron energy $E_{f_1} = 0.2$ and $E_{f_2} = 0.1$. We set the temperature $T = 0.02$ and the chemical potential $\mu = -5.52 \times 10^{-3}$ in the following numerical study. Then,

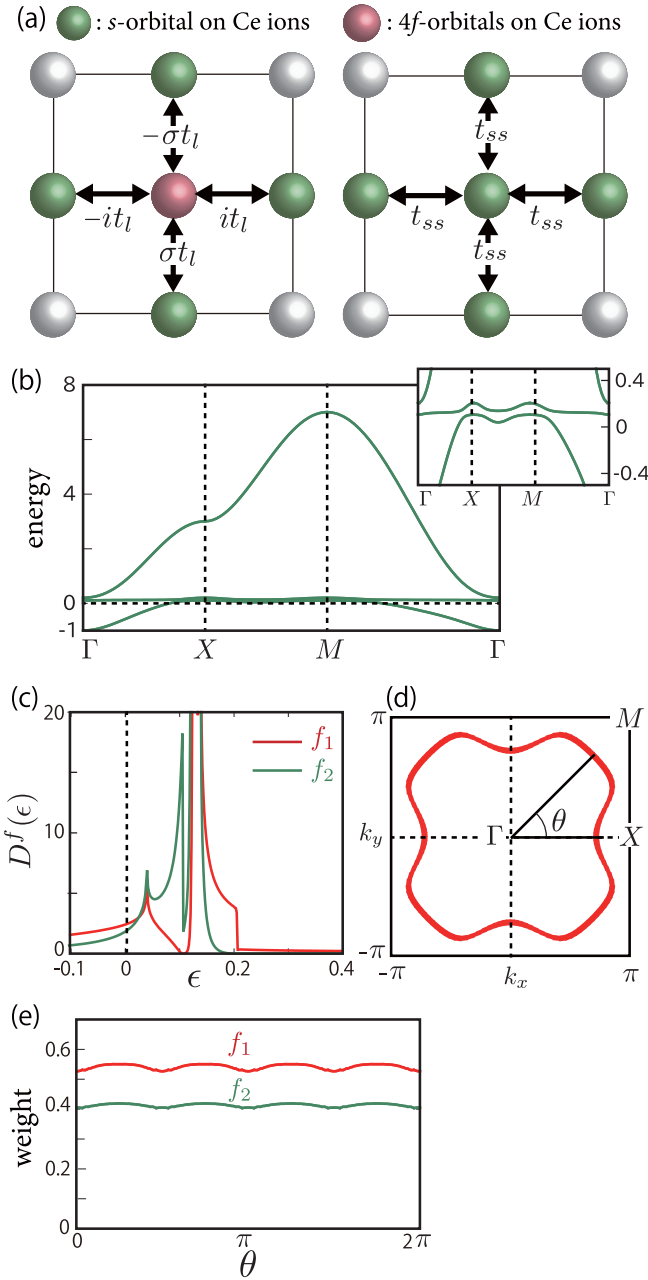


FIG. 1. (a) The nearest-neighbor-hopping integrals given by *s*-*s* and *s*-*f* hopping. $\sigma = 1(-1)$ for pseudospin up (down), $t_1 = -\sqrt{3}/14 t_{sf}$, $t_2 = -t_1/\sqrt{5}$. (b) Band dispersion along high-symmetry line. (c) Partial DoS of f_i electrons. The red (green) line corresponds to f_1 (f_2) orbital. (d) Obtained Fermi surface. (e) θ dependence of the f_i -orbital weight on Fermi surface. The red (green) line corresponds to f_1 (f_2) orbital.

f-electron number is $n_f = 0.9$, and *s*-electron number is $n_s = 0.3$.

In Fig. 1(b), we show the obtained band structure. $\epsilon = 0$ corresponds to the chemical potential. In the present three-band model, the lowest band crosses the Fermi level. The total band width is $W_D \sim 10$ (in unit $|t_{ss}| = 1$). $|t_{ss}|$ is of order 1 eV since $W_D \sim 10$ eV in CeCu₂Si₂ [28]. The width of quasiparticle band (=the lowest band) is $W_D^{\text{qp}} \sim 1$. Density of states (DoS) for f_i orbital; $D^{f_i}(\epsilon)$ is given in Fig. 1(c).

Here, the relation $D^{f_1}(0) \simeq D^{f_2}(0)$ is satisfied. In the present study, we neglect self energy. Figure 1(d) shows the obtained Fermi surface. In Fig. 1(e), we plot the θ dependence of the f_i -orbital weight, where θ is angle of the Fermi momentum defined in Fig. 1(d). We stress that the weights of f_1 and f_2 orbitals are comparable regardless of θ , which originates from the isotropic *s*-*f* hybridization given in Eq. (4) due to the strong SOI. (In contrast, in 3*d*-electron system such as Fe-based compounds, the *d*-orbital weight shows strong θ dependence.) This fact is favorable for the development of multiple higher-rank multipole susceptibilities, as we will show in Sec. IV.

If we consider the *f*-*f* hopping, the f_i -orbital weight comes to have θ dependence. Even in this case, the multiple higher-rank multipole susceptibilities can develop when $t_{ff} \ll t_{sf}$, which is naturally expected in heavy-fermion compounds. We will discuss this in more detail in Appendix D and in the future publication [45].

We introduce on-site Coulomb interactions in *f* electrons,

$$\hat{H}_U = u \cdot \frac{1}{4} \sum_{i,l'l'mm'} \sum_{\sigma\sigma'\rho\rho'} U_{ll'mm'}^{0,\sigma\sigma';\rho\rho'} f_{i l \sigma}^\dagger f_{i l' \sigma'} f_{i m \rho} f_{i m' \rho'}^\dagger, \quad (5)$$

where i is site index, and u is the value of Coulomb interaction. \hat{U}^0 is the interaction matrix normalized on the condition that $U_{11;11}^{0,\sigma\bar{\sigma};\sigma\bar{\sigma}} \equiv U^1 = 1$. Note that \hat{U}^0 in Eq. (5) is antisymmetrized.

Here, we derive \hat{U}^0 in Eq. (5) from the following L_z -basis Coulomb interaction:

$$\begin{aligned} \bar{U}_{l_z, l'_z, l''_z, l'''_z}^0 &= \frac{e^2}{4\pi\epsilon_0} \int d\vec{r} d\vec{r}' \frac{u_{l_z}^*(\vec{r}) u_{l'_z}^*(\vec{r}') u_{l''_z}(\vec{r}) u_{l'''_z}(\vec{r}')}{|\vec{r} - \vec{r}'|} \\ &= \sum_P a_{l_z, l'_z, l''_z, l'''_z}^P F^P, \end{aligned} \quad (6)$$

where $u_{l_z}(\vec{r}) (= R(r) \Theta_{l_z}(\theta) e^{i l_z \phi})$ is the wave function of the *f* electron with l_z in the absence of the SOI. F^P is the Slater integral introduced in Ref. [46], which is defined as $F^P = \frac{e^2}{4\pi\epsilon_0} \int dr \int dr' R^2(r) R^2(r') r_{\min}^P r_{\max}^{-(P+1)} r^2 r'^2$, where $r_{\min} = \min\{r, r'\}$ and $r_{\max} = \max\{r, r'\}$. In this paper, we put $(F^0, F^2, F^4, F^6) = (5.3, 9.09, 6.927, 4.756)$ in unit eV by referring Ref. [47]. Finally, we determine \hat{U}^0 in Eq. (5) by performing the unitary transformation of Eq. (6) and normalizing it on condition that $U^1 = 1$.

The present Coulomb interaction in Eq. (5) does not satisfy SU(2) symmetry in the pseudospin space. Nonetheless, the pseudospin is conserved in Eq. (5) for any value of a in Eq. (2). Equivalently, \hat{U}^0 satisfies the axial rotational symmetry along z axis. Then, \hat{U}^0 is uniquely decomposed into in-plane spin ($=s$), out-of-plane spin ($=s_\perp$), and charge ($=c$) channels as follows:

$$\begin{aligned} U_{ll'mm'}^{0;\sigma\sigma';\lambda\lambda'} &= \frac{1}{2} U_{ll'mm'}^{0;s} (\sigma_{\sigma\sigma'}^x \sigma_{\lambda'\lambda}^x + \sigma_{\sigma\sigma'}^y \sigma_{\lambda'\lambda}^y) \\ &\quad + \frac{1}{2} U_{ll'mm'}^{0;s_\perp} \sigma_{\sigma\sigma'}^z \sigma_{\lambda'\lambda}^z + \frac{1}{2} U_{ll'mm'}^{0;c} \sigma_{\sigma\sigma'}^0 \sigma_{\lambda'\lambda}^0, \end{aligned} \quad (7)$$

where $\vec{\sigma} = (\sigma^x, \sigma^y, \sigma^z)$ is Pauli matrix vector in the pseudospin space, and σ^0 is identity matrix. $\hat{U}^{0;ch}$ ($ch = s, s_\perp, c$)

TABLE I. Matrix elements of Coulomb interaction for in-plane spin channel (top left), out-of-plane spin channel (top right), and charge channel (bottom) for $l \neq m$. $J = J'$, $J^\perp = 0$, and $J^{x1} = -J^{x2}$ are satisfied in the present two-orbital model.

s	type	value	s_\perp	type	value
$U_{11;11}^{0;s}$	U^1	1.0	$U_{11;11}^{0;s_\perp}$	U^1	1.0
$U_{22;22}^{0;s}$	U^2	0.90	$U_{22;22}^{0;s_\perp}$	U^2	0.90
$U_{lm;lm}^{0;s}$	$U' - J + J^\perp$	0.80	$U_{lm;lm}^{0;s_\perp}$	$U' - J^{x1}$	0.68
$U_{ll;mm}^{0;s}$	$J - J^{x1}$	-0.12	$U_{ll;mm}^{0;s_\perp}$	J^\perp	0.0
$U_{lm;ml}^{0;s}$	$J' - J^{x2}$	0.20	$U_{lm;ml}^{0;s_\perp}$	$J' - J^{x2}$	0.20
c		type	value		
$U_{11;11}^{0;c}$		$-U^1$			-1.0
$U_{22;22}^{0;c}$		$-U^2$			-0.90
$U_{lm;lm}^{0;c}$		$U' - J - J^\perp$			0.80
$U_{ll;mm}^{0;c}$		$J - 2U' + J^{x1}$			-1.5
$U_{lm;ml}^{0;c}$		$-J' + J^{x2}$			-0.20

is defined as

$$\begin{aligned}
\hat{U}^{0;s} &= \hat{U}^{0;\uparrow\uparrow;\uparrow\uparrow} - \hat{U}^{0;\uparrow\uparrow;\downarrow\downarrow} \\
\hat{U}^{0;s_\perp} &= \hat{U}^{0;\uparrow\downarrow;\uparrow\downarrow} \\
\hat{U}^{0;c} &= \hat{U}^{0;\uparrow\uparrow;\uparrow\uparrow} + \hat{U}^{0;\uparrow\uparrow;\downarrow\downarrow}.
\end{aligned} \tag{8}$$

The matrix elements of $\hat{U}^{0;ch}$ ($ch = s, s_\perp, c$) are summarized in Table I. Each element is composed of the intraorbital Coulomb interaction U , interorbital U' , exchange interactions J, J^\perp, J', J^{x1} , and J^{x2} . The definition and numerical value of each component are given in Appendix B. In the case of $a = 1$ and $b = 0$, the other elements not listed in the Table I become zero. Although some of these elements (e.g., $U_{11;12}^{0;ch}$) come to be finite for $a \lesssim 1$, they remain very small and negligible. Therefore Table I is still useful, practically. Note that $a = \sqrt{5/6}$ and $b = \sqrt{1/6}$ are satisfied in cubic symmetry.

In the present two-orbital model in Eq. (2), there are 16-type active multipole operators up to rank 5; monopole (rank 0), dipole (rank 1), quadrupole (rank 2), octupole (rank 3), hexadecapole (rank 4), and dotriacontapole (rank 5) moment as shown in Table II [13]. Some operators belong to the same irreducible representation (IR). Since the system is inversion symmetric, an even-rank (odd-rank) operator corresponds to an electric (magnetic) multipole operator. Each multipole operator of rank k are composed of 4×4 tensor $J_q^{(k)}$ ($q = -k \sim k$) [8,48], which is given by

$$[J_\pm, J_q^{(k)}] = \sqrt{(k \mp q)(k \pm q + 1)} J_{q\pm 1}^{(k)}, \tag{9}$$

$$J_k^{(k)} = (-1)^k \sqrt{\frac{(2k-1)!!}{(2k)!!}} J_+^k. \tag{10}$$

By using $J_q^{(k)}$, we obtain 4×4 multipole operators \hat{O}^Q . Here, $Q \equiv (\Gamma, \phi)$, where Γ is index of the irreducible representation

TABLE II. Irreducible representation and 16-type active multipole operators in the present two-orbital model. Operator with rank k corresponds to 2^k pole. N_Γ is the number of operators in symmetry Γ . Each operator is classified into the pseudospin or charge channel, ch_Γ .

IR (Γ)	rank (k)	Operator (Q)	N_Γ	ch_Γ
	0	$\hat{1}$		
A_1^+	2	\hat{O}_{20}	3	c
	4	\hat{H}_0		
A_2^+	4	\hat{H}_z	1	s
E^+	2	$\hat{O}_{yz}, \hat{O}_{zx}$	2	s_\perp
A_1^-	5	\hat{D}_4	1	c
	1	\hat{J}_z		
A_2^-	3	\hat{T}_z	3	s
	5	\hat{D}_z		
	1	\hat{J}_x, \hat{J}_y		
E^-	3	\hat{T}_x, \hat{T}_y	6	s_\perp
	5	\hat{D}_x, \hat{D}_y		

($\Gamma = A_1^+, A_2^+, E^+, A_1^-, A_2^-, E^-$) and ϕ is index of independent multipole operator ($\phi = 1 \sim N_\Gamma$). For each Γ , N_Γ is given in Table II. The matrix representations for 16-type operators are given in Appendix C.

Here, we introduce the effective on-site electric multipole-multipole interaction \hat{V}^{ph} that belongs to A_1^+ symmetry (=identical representation),

$$\begin{aligned}
V_{ll'mm'}^{\text{ph}} &= 2g W_{ll'mm'} \\
&= 2g (\hat{C}^{A_1^+})_{ll'} (\hat{C}^{A_1^+})_{mm'},
\end{aligned} \tag{11}$$

where $\hat{C}^{A_1^+}$ is the dimensionless matrix given by a linear combination of multipole operators belong to $\Gamma = A_1^+$ in Table II. It is expressed as

$$\hat{C}^{A_1^+} \equiv \alpha \hat{\tau}^0 + \beta \hat{\tau}^z + \gamma \hat{\tau}^x, \tag{12}$$

where $\hat{\tau}^\mu$ ($\mu = x, y, z$) is Pauli matrix in the orbital basis (f_1, f_2), and $\hat{\tau}^0$ is identity matrix. In the presence of g , the Coulomb interaction $u\hat{U}^{0;c}$ is replaced with $u\hat{U}^{0;c} + 2g\hat{W}$. In the present numerical study, we put $(\alpha, \beta, \gamma) = (0, 1, -1)$. We verified that the main results are qualitatively same as those of $(\alpha, \beta, \gamma) = (0, 1, 1)$. The numerical results are not sensitive to the ratio of (α, β, γ) .

This effective interaction can be induced by (for instance) the electron-phonon interaction due to A_1^+ mode, such as the oscillation of c -axis length [49]. In this case, g is expressed as $g = \tilde{g} \frac{\omega_D^2}{\omega_D + \omega_j^2}$, where $\tilde{g} = \frac{2\eta^2}{\omega_D}$ (> 0): ω_D is the phonon frequency, η is the coupling constant between electrons and phonon, and $\omega_j = 2j\pi T$ is the Boson Matsubara frequency. In the present study, we drop ω_j dependence of g for simplicity. That is, we neglect the retardation effect, which leads to underestimation of the s -wave superconducting T_c as discussed in Ref. [35]. The A_1^+ effective interaction in Eq. (11) is classified into even-rank multipole interaction. Therefore, strong electric (=even-rank) multipole fluctuations are

induced by the interaction g . On the other hand, the magnetic (=odd-rank) multipole susceptibilities are independent of g .

III. GREEN FUNCTION

Here, we introduce the Green functions in the present model. The 3×3 matrix form of the Green function is given by

$$\hat{G}^\sigma(\mathbf{k}, i\epsilon_n) = ((i\epsilon_n - \mu)\hat{1} - \hat{h}_\mathbf{k}^\sigma)^{-1}, \quad (13)$$

where $\hat{h}_\mathbf{k}^\sigma$ is introduced in Eq. (3). The first two rows and columns of Eq. (13) give the f -orbital Green functions. They are expressed as

$$G_{lm}^{f,\sigma}(k) = G_l^{0f}(k)\delta_{lm} + G_l^{0f}(k)V_{kl\sigma}^* G^{c,\sigma}(k)V_{km\sigma} G_m^{0f}(k), \quad (14)$$

where $l, m = 1, 2, k = (\mathbf{k}, \epsilon_n) = (\mathbf{k}, (2n+1)\pi T)$, and

$$G_l^{0f}(k) = (i\epsilon_n - \mu - E_l)^{-1}. \quad (15)$$

$G^{c,\sigma}(k)$ is the s -electron Green function given by the (3,3) component of Eq. (13). It is expressed as

$$G^{c,\sigma}(k) = \left(i\epsilon_n - \mu - \epsilon_k - \sum_l V_{kl\sigma} G_l^{0f}(k) V_{kl\sigma}^* \right)^{-1}. \quad (16)$$

In the present two-orbital model, the relation $V_{kl\uparrow}^* V_{km\uparrow} = V_{kl\downarrow}^* V_{km\downarrow}$ is satisfied, as we can verify from Eq. (4). For this reason, the Green functions become independent of spin index:

$$\begin{aligned} G_{lm}^f(k) &\equiv G_{lm}^{f,\uparrow}(k) = G_{lm}^{f,\downarrow}(k), \\ G^c(k) &\equiv G^{c,\uparrow}(k) = G^{c,\downarrow}(k). \end{aligned} \quad (17)$$

In the present model, diagonal ($l = m$) components of $G_{lm}^f(k)$ and off-diagonal ($l \neq m$) ones are comparable since each s - f hybridization in Eq. (4) is isotropic in magnitude. It is a characteristic feature of the multiorbital f -electron systems.

IV. SUSCEPTIBILITY

First, we perform the random phase approximation (RPA) in order to obtain the f -electron susceptibility. In this calculation, we use 32×32 \mathbf{k} -meshes and 128 Matsubara frequencies. The irreducible susceptibility of f electron is given by

$$\chi_{ll'mm'}^0(q) = -T \sum_k G_{lm}^f(k+q) G_{m'l'}^f(k), \quad (18)$$

where $q = (\mathbf{q}, \omega_j) = (\mathbf{q}, 2j\pi T)$. In the RPA, the susceptibility for each channel (ch) is given as

$$\hat{\chi}^{ch}(q) = \hat{\chi}^0(q)(\hat{1} - u\hat{U}^{0;ch}\hat{\chi}^0(q))^{-1}, \quad (19)$$

where $\hat{\chi}^{ch}(q)$ is $2^2 \times 2^2$ matrix. Using $\hat{\chi}^{ch}$ ($ch = s, s\perp, c$), the f -electron susceptibility in the $L = (l, \sigma)$ basis is expressed as

$$\begin{aligned} \hat{\chi}^{\sigma\sigma'\lambda\lambda'} &= \frac{1}{2}\hat{\chi}^s(\sigma_{\sigma\sigma'}^x \sigma_{\lambda\lambda'}^x + \sigma_{\sigma\sigma'}^y \sigma_{\lambda\lambda'}^y) \\ &+ \frac{1}{2}\hat{\chi}^{s\perp} \sigma_{\sigma\sigma'}^z \sigma_{\lambda\lambda'}^z + \frac{1}{2}\hat{\chi}^c \sigma_{\sigma\sigma'}^0 \sigma_{\lambda\lambda'}^0. \end{aligned} \quad (20)$$

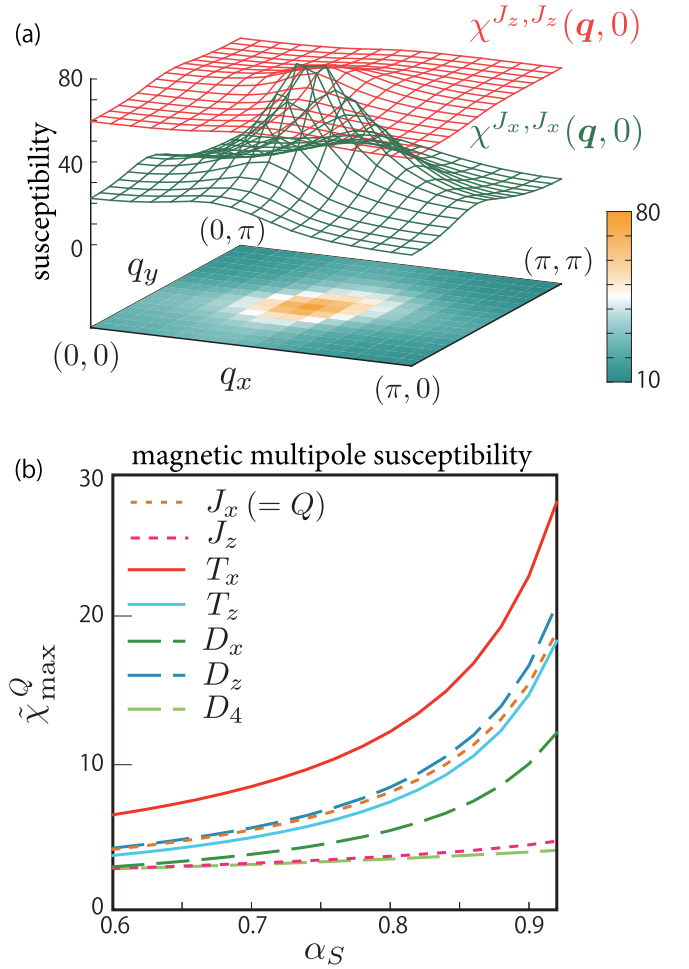


FIG. 2. (a) \mathbf{q} dependence of the magnetic dipole susceptibility. $\chi^{J_z, J_z}(\mathbf{q}, 0) \gg \chi^{J_x, J_x}(\mathbf{q}, 0)$ is satisfied at $\mathbf{q} = (0, 0)$. (b) α_S dependence of magnetic multipole susceptibility. Higher-rank magnetic multipole susceptibilities are strongly enlarged.

Here, we define the pseudospin Stoner factor α_S ($\alpha_{S\perp}$) as the largest eigenvalue of $u\hat{U}^{0;s(s\perp)}\hat{\chi}^0(q)$. In the present model, each matrix element of $\hat{U}^{0;s}$ and that of $\hat{U}^{0;s\perp}$ in Table I are the same except for $(lmlm)$ and $(llmm)$ elements. For this reason, $\hat{\chi}^s \approx \hat{\chi}^{s\perp}$ and $\alpha_S \approx \alpha_{S\perp}$ are satisfied.

Now, we define the multipole susceptibility for $Q(= (\Gamma, \phi))$,

$$\chi^{Q, Q'}(q) = \int_0^\beta d\tau \mathcal{O}^Q(\mathbf{q}, \tau) \mathcal{O}^{Q'}(-\mathbf{q}, \tau) e^{i\omega_j \tau}, \quad (21)$$

where $\mathcal{O}^Q(\mathbf{q}, \tau) = \sum_{L, M, k} O_{L, M}^Q f_{km\sigma}^\dagger(\tau) f_{k+q\sigma'}(\tau)$. In 3D models, $\chi^{(\Gamma, \phi), (\Gamma', \phi')}(q)$ can be finite even in the case of $\Gamma \neq \Gamma'$. In contrast, in the present 2D model, $\chi^{(\Gamma, \phi), (\Gamma', \phi')}(q) = 0$ for any q in the case of $\Gamma \neq \Gamma'$, which is a great merit of the present model in analysis. Note that $\chi^{(\Gamma, \phi), (\Gamma', \phi')}(q)$ for $\Gamma = A_1^+, A_2^+, E^+$ is classified into electric susceptibility, and that for $\Gamma = A_1^-, A_2^-, E^-$ is classified into magnetic susceptibility. In the present model, α_S corresponds to the A_2^- magnetic (=odd-rank) susceptibility, that is, $\alpha_S = \alpha_{A_2^-}$ in the RPA. We obtain the relation $1 \gtrsim \alpha_{A_2^-} \gtrsim \alpha_{E^-}$.

In Fig. 2(a), we show obtained susceptibilities at $u = 0.31$ for the magnetic dipole $J_z = (A_2^-, 1)$, $\chi^{J_z, J_z}(\mathbf{q}, 0)$, and $J_x = (E^-, 1)$, $\chi^{J_x, J_x}(\mathbf{q}, 0)$. In this case, $\alpha_S = 0.90$. Note that $\chi^{J_x, J_x} = \chi^{J_y, J_y}$. We find that $\chi^{J_z, J_z}(\mathbf{q}, 0)$ is much larger than $\chi^{J_x, J_x}(\mathbf{q}, 0)$ at $\mathbf{q} = (0, 0)$ while they are almost the same around the peak at $\mathbf{q} \simeq (\pi/2, \pi/2)$. Thus the uniform magnetic susceptibility shows strong Ising anisotropy, which is actually observed in CeCu_2Si_2 .

Hereafter, to compare among different-rank of multipole susceptibilities, we define normalized multipole operator $\hat{\mathcal{O}}^Q$ as $\text{Tr}(\hat{\mathcal{O}}^Q) = 1$, that is,

$$\hat{\mathcal{O}}^Q = \hat{\mathcal{O}}^Q / \sqrt{\text{Tr}(\hat{\mathcal{O}}^Q)}. \quad (22)$$

The normalized susceptibility $\tilde{\chi}^{Q, Q'}(q)$ is given by replacing $\hat{\mathcal{O}}^Q$ in Eq. (21) with $\hat{\mathcal{O}}^Q$. In Fig. 2(b), we show α_S dependencies of the maximum of magnetic multipole susceptibilities $\tilde{\chi}_{\max}^Q \equiv \max_{\mathbf{q}} \{\tilde{\chi}^{Q, Q}(\mathbf{q}, 0)\}$. α_S linearly increases in proportion to u . The obtained $\tilde{\chi}_{\max}^Q$ is the most divergent for $Q = T_x$. This fact is consistent with the RPA result based on the first-principles model in Ref. [28]. Secondly, $\tilde{\chi}_{\max}^Q$ for $Q = D_z, J_x, T_z, D_4$ is also strongly enlarged. Therefore various magnetic multipole (including higher-rank) susceptibilities are simultaneously enlarged in the RPA. This is a characteristic feature of f -electron systems with strong SOI [13]. We find that the inter-rank magnetic multipole susceptibilities, such as $\tilde{\chi}^{J_z, T_z}$, are also enlarged.

Now, we explain the reason why higher-rank magnetic multipole susceptibilities are enlarged. Our result means that orbital-off-diagonal components of $\chi_{ll'mm'}^S$ are comparable to orbital-diagonal ones. In fact, $\chi_{1111}^S \approx \chi_{1112}^S$ is satisfied in the present model. It originates from the fact that each s - f hybridization in Eq. (4) is isotropic in the x and y directions due to the strong SOI, and therefore each f_i -orbital weight is independent of θ as shown in Fig. 1(e). This is the origin of the large orbital-off-diagonal components of G_{lm}^f and those of $\chi_{ll'mm'}^{s(\pm)}$. This situation is quite different from $3d$ -electron systems, in which off-diagonal components of \hat{G} and $\hat{\chi}^s$ remain small in general.

Finally, we comment on electric (=even-rank) susceptibilities obtained by the RPA. In the absence of electric multipole-multipole (phonon-induced) interaction: $g = 0$, the obtained electric susceptibilities are much smaller than magnetic ones. That is, charge stoner factor α_C , which is defined as the largest eigenvalue of $(u\hat{U}^{0;c} + 2g\hat{W})\hat{\chi}^0(q)$, satisfy $\alpha_C \ll \alpha_S$. In the present model, $(\alpha_C, \alpha_S) = (0.55, 0.90)$. On the other hand, the hexadecapole χ^{H_0, H_0} and quadrupole $\chi^{O_{20}, O_{20}}$ susceptibility are enlarged at $q \approx (\pi, \pi)$ when we consider the small g (> 0). In this case, α_C increases to 0.84 at $g = 0.04$. Note that the obtained electric susceptibilities work as attractive interaction for s -wave superconductivity, as we will explain in the following section.

In principle, some experimental signatures due to the electric multipole susceptibility can be observed. The enhancement of χ^c at $\mathbf{q} \neq \mathbf{0}$ obtained in the present model may cause the softening of phonon dispersion, which is observable by using (for instance) neutron scattering experiment.

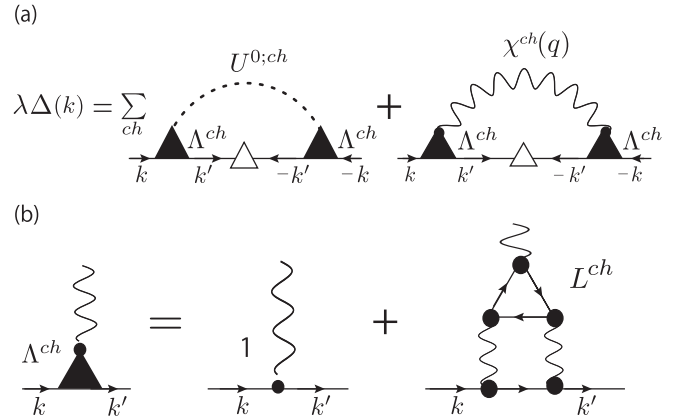


FIG. 3. (a) Linearized gap equation in the present study. The black triangle shows three-point vertex correction (U -VC). (b) U -VC due to the AL process.

V. GAP EQUATION

Now, we solve the linearized gap equation by focusing on the important roles of the vertex corrections, which we call U -VC. The bare electron-boson couplings are dressed by the U -VC, which is totally dropped in conventional Migdal approximation. The gap equation for spin-singlet pairing in the band basis is given as

$$\lambda \Delta(\mathbf{k}, \epsilon_n) = -\frac{\pi T}{(2\pi)^2} \sum_{\epsilon_m} \oint_{FS} \frac{d\mathbf{k}'}{v_{\mathbf{k}'}} \frac{\Delta(\mathbf{k}', \epsilon_m)}{|\epsilon_m|} V_{k,k'}^{\text{sing}}, \quad (23)$$

where $\Delta(\mathbf{k}, \epsilon_n)$ is the gap function on Fermi surface, λ is the eigenvalue, and $v_{\mathbf{k}}$ is the Fermi velocity on Fermi surface. $V_{k,k'}^{\text{sing}}$ is the spin singlet pairing interaction including U -VC. The diagrammatic expression of the gap equation is shown in Fig. 3(a). The black triangle shows the three-point vertex correction due to many body effects. We consider the AL-type diagram for U -VC given in Fig. 3(b), which is explained in more detail in Sec. VI. The pairing interaction in Eq. (23) is obtained by

$$\begin{aligned} V_{k,k'}^{\text{sing}} &= V_{k,k'}^{udud} - V_{k,k'}^{uudd} \\ &= \frac{1}{2} \sum_{\Sigma, \Lambda} V_{k,k'}^{\Sigma \Lambda \bar{\Sigma}} (1 - 2\delta_{\Sigma \Lambda}), \end{aligned} \quad (24)$$

where $\Sigma, \Lambda = u$ (d) is pseudospins up (down) that denotes the Kramers doublet of the Bloch function, and $\bar{\Sigma} \equiv -\Sigma$. $V_{k,k'}^{\Sigma \Lambda \bar{\Sigma}}$ is given as

$$\begin{aligned} V_{k,k'}^{\Sigma \Lambda \bar{\Sigma}} &= \sum_{ll'mm'} \sum_{\sigma\sigma'\lambda\lambda'} U_{l\sigma}^{\Sigma*}(\mathbf{k}) U_{m'\lambda'}^{\bar{\Sigma}*}(-\mathbf{k}) \\ &\quad \times V_{ll'mm'}^{\sigma\sigma'\lambda\lambda'}(k, k') U_{m\lambda}^{\bar{\Sigma}}(-\mathbf{k}') U_{l'\sigma'}^{\Lambda}(\mathbf{k}'), \end{aligned} \quad (25)$$

where $U_{l\sigma}^{\Sigma}(\mathbf{k})$ is the unitary matrix connecting between $f_{kl\sigma}^{\dagger}$ and the quasiparticle creation operator $f_{k\Sigma}^{\dagger}$. In the presence of the time-reversal symmetry, $U_{l\sigma}^{\Sigma}(\mathbf{k})$ is related to $U_{l\sigma}^{\bar{\Sigma}}(\mathbf{k})$ as $U_{l\sigma}^{\Sigma}(-\mathbf{k}) = (-1)^{\delta_{\Sigma\sigma} + 1} U_{l\sigma}^{\bar{\Sigma}}(\mathbf{k})^*$ [50]. $V_{ll'mm'}^{\sigma\sigma'\lambda\lambda'}(k, k')$ is the pairing interaction in the orbital basis introduced in Sec. VI. In the present model, there is rotational symmetry along z axis in the pseudospin space. For this reason, $V_{ll'mm'}^{\sigma\sigma'\lambda\lambda'}(k, k')$

is uniquely decomposed into spin and charge channels as follows:

$$V_{ll'mm'}^{\sigma\sigma'\lambda\lambda'} = \frac{1}{2}V_{ll'mm'}^{s\perp}(\sigma_{\sigma\sigma'}^x\sigma_{\lambda'\lambda}^x + \sigma_{\sigma\sigma'}^y\sigma_{\lambda'\lambda}^y) + \frac{1}{2}V_{ll'mm'}^s\sigma_{\sigma\sigma'}^z\sigma_{\lambda'\lambda}^z + \frac{1}{2}V_{ll'mm'}^c\sigma_{\sigma\sigma'}^0\sigma_{\lambda'\lambda}^0, \quad (26)$$

where we drop the first-order term ($U^{0;s\perp}$) from $V^{0;s\perp}$ in order to avoid double counting [36]. From Eqs. (24)–(26), we obtain that

$$V_{k,k'}^{\text{sing}} = \sum_{ll'mm'} V_{ll'mm'}^{s\perp}(\hat{A}_{\uparrow\downarrow\uparrow\downarrow}^{udud} - \hat{A}_{\uparrow\downarrow\uparrow\downarrow}^{uddu})_{ll'mm'} + \frac{1}{2}V_{ll'mm'}^c(\hat{A}_{\uparrow\uparrow\uparrow\uparrow}^{udud} + \hat{A}_{\uparrow\downarrow\downarrow\downarrow}^{udud} - \hat{A}_{\uparrow\uparrow\uparrow\uparrow}^{uddu} - \hat{A}_{\uparrow\downarrow\downarrow\downarrow}^{uddu})_{ll'mm'} + \frac{1}{2}V_{ll'mm'}^s(\hat{A}_{\uparrow\uparrow\uparrow\uparrow}^{udud} - \hat{A}_{\uparrow\downarrow\downarrow\downarrow}^{udud} - \hat{A}_{\uparrow\uparrow\uparrow\uparrow}^{uddu} + \hat{A}_{\uparrow\downarrow\downarrow\downarrow}^{uddu})_{ll'mm'}, \quad (27)$$

where

$$(\hat{A}_{\sigma\sigma'\lambda\lambda'}^{\Sigma\bar{\Sigma}\bar{\Lambda}\Lambda})_{ll'mm'} \equiv U_{l\sigma}^{\Sigma*}(\mathbf{k})U_{m\sigma'}^{\bar{\Sigma}*}(-\mathbf{k})U_{m\lambda}^{\bar{\Lambda}}(-\mathbf{k}')U_{l\lambda'}^{\Lambda}(\mathbf{k}').$$

In the present model, the electric multipole paring interaction corresponds to attraction, while the magnetic one corresponds to repulsion. To understand this fact, we consider the paring interaction in the absence of SOI, like in 3d-electron systems. In this case, we can put $U_{l\sigma}^{\Sigma*}(\mathbf{k}) = U_{l\sigma}^*(\mathbf{k})\delta_{\Sigma,\sigma}$ and

$$\begin{aligned} \hat{A}_{\uparrow\downarrow\uparrow\downarrow}^{udud} &= \hat{A}_{\uparrow\downarrow\uparrow\downarrow}^{uddu} \neq 0 \\ \hat{A}_{\uparrow\downarrow\uparrow\downarrow}^{uddu} &= \hat{A}_{\uparrow\uparrow\uparrow\uparrow}^{udud} = \hat{A}_{\uparrow\downarrow\downarrow\downarrow}^{udud} = \hat{A}_{\uparrow\uparrow\uparrow\uparrow}^{uddu} = 0 \end{aligned}$$

Then, we obtain the following simple expression:

$$V_{k,k'}^{\text{no-SOI}} = \sum_{ll'mm'} (\hat{V}^{s\perp} + \frac{1}{2}\hat{V}^s - \frac{1}{2}\hat{V}^c)_{ll'mm'}(\hat{A}_{\uparrow\downarrow\uparrow\downarrow}^{udud})_{ll'mm'},$$

where $V^{s\perp} = V^s$ is satisfied when SOI is dropped. Thus $V_{k,k'}^{\text{sing}}$ in Eq. (27) is reduced to the well-known expression $V_{k,k'}^{\text{no-SOI}} \propto \frac{3}{2}V^s - \frac{1}{2}V^c$. In conclusion, the charge- or electric-channel paring interaction works as attraction, while the spin- or magnetic-channel one works as repulsion.

VI. IMPORTANT ROLES OF U -VC

Here, we discuss the important roles of U -VC in the paring interaction. Until now, U -VC in d -electron systems has been studied intensively by some theoretical methods, such as the functional renormalization group (fRG) theory and perturbation theory. Both theoretical frameworks reveal that U -VC makes significant contribution to the superconductivity, especially in multiorbital systems, so Migdal approximation fails. In more detail, AL-type U -VC becomes more important than MT type one near the magnetic QCP. However, U -VC in f -electron system with strong SOI has not been understood at all. In the present study, we show that U -VC in f -electron systems is more important than that in d -electron systems due to large SOI.

Now, we discuss the paring interaction with U -VC. In the present model, U -VC satisfy the pseudospin conservation. Thus the paring interaction for each channel in Eq. (27) is expressed as

$$\hat{V}^{ch}(k, k') = \hat{\Lambda}_{k,k'}^{ch}\hat{I}^{ch}(k - k')\hat{\Lambda}_{-k,-k'}^{ch}, \quad (28)$$

where

$$\hat{I}^{ch}(k - k') = u^2\hat{U}^{0;ch}\hat{\chi}^{ch}(k - k')\hat{U}^{0;ch} + u\hat{U}^{0;ch}. \quad (29)$$

Here, $\hat{\Lambda}_{k,k'}^{ch}$ is an enhancement factor for electron-boson coupling given by

$$(\hat{\Lambda}_{k,k'}^{ch})_{ll'mm'} = \delta_{lm}\delta_{l'm'} + (\hat{L}_{k,k'}^{ch})_{ll'mm'}, \quad (30)$$

where $\hat{L}_{k,k'}^{ch}$ is AL-type U -VC, whose diagrammatic expression is given in Fig. 3(b). In Eq.(28), $(\hat{\Lambda}_{k,k'}^{ch})_{ll'mm'} \equiv (\hat{\Lambda}_{k,k'}^{ch})_{m'm'l'l}$. In the present model, the MT-type U -VC is negligible compared to AL-type one. For this reason, we calculate only AL-type U -VC. Note that $\hat{V}^{ch} = \hat{I}^{ch}$ in the Migdal approximation ($\hat{\Lambda}^{ch} = \hat{1}$).

Hereafter, we discuss only the charge-channel U -VC $\hat{\Lambda}_{k,k'}^c$ since it becomes much larger than unity near the magnetic QCP, whereas spin-channel one remains order of unity. Hence, the charge-channel paring interaction is enlarged by $\hat{\Lambda}_{k,k'}^c$. Here, $\hat{L}_{k,k'}^c$ is derived from the U -VC in the (l, σ) basis:

$$\hat{L}_{k,k'}^c \equiv \hat{L}_{k,k'}^{\uparrow\uparrow\uparrow\uparrow} + \hat{L}_{k,k'}^{\uparrow\uparrow\downarrow\downarrow} = \hat{L}_{k,k'}^{\downarrow\downarrow\downarrow\downarrow} + \hat{L}_{k,k'}^{\downarrow\downarrow\uparrow\uparrow}, \quad (31)$$

whose Feynman diagram is shown in Fig. 4(a). The analytic expression of $\hat{L}_{k,k'}^c$ is given as

$$\begin{aligned} (\hat{L}_{k,k'}^c)_{ll'mm'} &= \frac{T}{2} \sum_{p,abcdef} B_{abcdef}^{mm'}(k - k', p) \\ &\times \sum_{ch} a^{ch} I_{lacd}^{ch}(k - k' + p) I_{bl'ef}^{ch}(-p), \end{aligned} \quad (32)$$

where $(a^s, a^{s\perp}a^c) = (1, 2, 1)$, and

$$\begin{aligned} B_{abcdef}^{mm'}(q, p) &\equiv \frac{1}{4}G_{ab}^f(k' - p) \\ &\times \{C_{cdef}^{mm'}(q, p) + C_{efcd}^{mm'}(q, q + p)\}, \end{aligned} \quad (33)$$

$$C_{cdef}^{ab}(q, p) \equiv -T \sum_{k'} G_{ca}^f(k' + q) G_{bf}^f(k') G_{ed}^f(k' - p). \quad (34)$$

Here, $a \sim f$ are orbital indices. In the present numerical study, we put $g = 0$ in the $\hat{L}_{k,k'}^{ch}$, since the contribution from χ^c is negligibly smaller than that from χ^s and $\chi^{s\perp}$ [35].

Next, we show numerical results of $\hat{\Lambda}_{k,k'}^c$. Here, we use 16×16 \mathbf{k} meshes and 128 Matsubara frequencies. In Figs. 4(b) and 4(c), we show the α_S dependence of maximum value of $\hat{\Lambda}_{k,k'}^c$ on the Fermi surface,

$$\Lambda_{ll'mm'}^{c,\text{max}} \equiv \max_{\mathbf{k}, \mathbf{k}' \in FS} |(\hat{\Lambda}_{k,k'}^c)_{ll'mm'}|, \quad (35)$$

at $\epsilon_n = \epsilon_{n'} = \pi T$. We plot various orbital components of U -VC. Note that the other elements are obtained by using the symmetry relation of orbital indices, that is, $\Lambda_{ll'mm'}^{c,\text{max}} = \Lambda_{l'l'm'm'}^{c,\text{max}}$. We find that they work as large enhancement factors for the coupling constant between electrons and charged-bosons ($|\hat{\Lambda}^c| \gg 1$) near the magnetic QCP ($\alpha_S \lesssim 1$). Note that all magnetic multipole susceptibilities except for D_4 , $Q = (A_1^-, 1)$, are included in either χ^s or $\chi^{s\perp}$. This behavior originates from the relation $\hat{\Lambda}_{k,k'}^c \propto \sum_p \hat{\chi}^s(k - k' + p)\hat{\chi}^s(p) + 2\hat{\chi}^{s\perp}(k - k' + p)\hat{\chi}^{s\perp}(p)$. This is qualitatively similar to d -electron systems without SOI as shown in Fig. 2(c) in

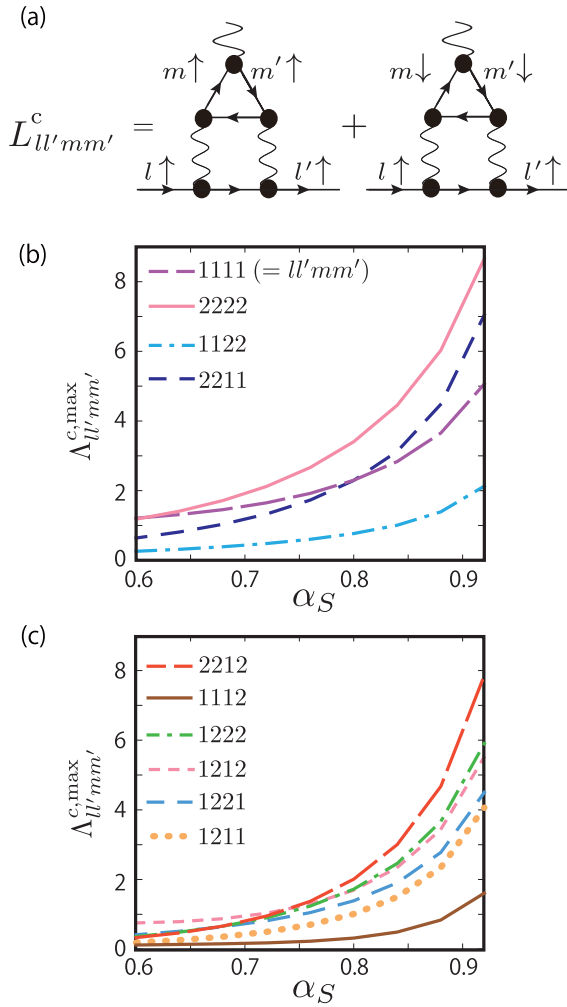


FIG. 4. (a) Charge-channel U -VC given by AL process. Only the diagrams given by the first term of \hat{B} in Eq. (33) are shown. [(b) and (c)] α_S dependence of charge-channel U -VC $\Lambda_{ll'mm'}^{c,\max}$. Various orbital components are strongly enlarged.

Ref. [35]. In conclusion, U -VC in f -electron systems give significant contribution as well as in d -electron systems.

We stress that there are some significant differences from d -electron systems. In fact, in the present f -electron system, (i) various orbital components of U -VC are equally enlarged, and (ii) the magnitude of U -VC are even larger than in d -electron systems at the same α_S . These results originate from multiple (higher-rank) magnetic multipole fluctuations as shown in Fig. 2(b). To clarify this fact, we are going to elucidate what types of multipole fluctuations are significant for U -VC below. We recall that the f -electron susceptibility in Eq. (20) is uniquely expanded on the basis of 4×4 matrix expression of multipole operator $\hat{O}^Q (= \hat{O}^{(\Gamma,\phi)})$ given in Appendix C as follows:

$$\chi_{LL'MM'}(q) = \sum_{\Gamma,\phi,\phi'} a^{\Gamma,\phi,\phi'}(q) O_{LL'}^{(\Gamma,\phi)} O_{MM'}^{(\Gamma,\phi)*}. \quad (36)$$

Note that $\sum_{LL'} O_{LL'}^{(\Gamma,\phi)} O_{LL'}^{(\Gamma,\phi)*} = 0$ for $\Gamma \neq \Gamma'$. The derivation of the coefficient $a^{\Gamma,\phi,\phi'}(q)$ is explained in Appendix D. In the same way, the interaction $\hat{I} (= u^2 \hat{U}^0 \hat{\chi}^{ch} \hat{U}^0 + u \hat{U}^0)$ in the

$L = (l, \sigma)$ basis is expanded as

$$I_{LL'MM'} = \sum_{\Gamma,\phi,\phi'} b^{\Gamma,\phi,\phi'}(q) O_{LL'}^{(\Gamma,\phi)} O_{MM'}^{(\Gamma,\phi)*}. \quad (37)$$

By utilizing the pseudospin conservation law, each term in the right-hand-side of Eq. (37) is expressed in the l basis as $I_{ll'mm'}^{ch,\Gamma,\phi,\phi'}$. Note that $\hat{I}^{ch,\Gamma,\phi,\phi'} = 0$ for $ch \neq ch_\Gamma$. By replacing $I_{ll'mm'}^{ch}$ in Eq. (32) with $I_{ll'mm'}^{ch,Q} (\equiv I_{ll'mm'}^{ch,\Gamma,\phi,\phi'})$, we obtain multipole-decomposed U -VC symbolically expressed as

$$(\hat{L}_{k,k'}^{c,QQ}) = \frac{T}{2} \sum_{ch} \hat{B} \hat{I}^{ch,Q} \hat{I}^{ch,Q}, \quad (38)$$

$$(\hat{L}_{k,k'}^{c,QQ'}) = \frac{T}{2} \sum_{ch} \hat{B} (\hat{I}^{ch,Q} \hat{I}^{ch,Q'} + \hat{I}^{ch,Q'} \hat{I}^{ch,Q}). \quad (39)$$

where $Q \neq Q'$. The diagrammatic expression of Eq. (39) is given in Fig. 5(a). Note that the relation $\hat{L}^c \approx \sum_{\{Q,Q'\}} \hat{L}^{c,QQ'}$ is satisfied. $\hat{L}^{c,QQ'}$ is given by

$$(\hat{L}_{k,k'}^{c,QQ'})_{ll'mm'} = \delta_{lm} \delta_{l'm'} + (\hat{L}_{k,k'}^{c,QQ'})_{ll'mm'}. \quad (40)$$

In Figs. 5(b)–5(e), we show the maximum of multipole-decomposed U -VC defined as

$$\Lambda_{ll'mm'}^{c,QQ'} \equiv \max_{k,k' \in FS} |(\hat{L}_{k,k'}^{c,QQ'})_{ll'mm'}| \quad (41)$$

at $\epsilon_n = \epsilon_{n'} = \pi T$. We consider only odd-rank (=magnetic) multipole operators for Q and Q' since the contributions from even-rank multipole operators are negligibly small in RPA. In addition, $\hat{L}_{ll'mm'}^{c,QQ'}$ with $Q = (\Gamma, \phi)$ and $Q' = (\Gamma', \phi')$ becomes zero except for $\Gamma = \Gamma'$ in the present model. Figures 5(b) and 5(c) show the orbital-diagonal component of U -VC given by $\Lambda_{2222}^{c,QQ'}$. It becomes the largest for $(Q, Q') = (T_x, T_x)$. Subsequently, $(Q, Q') = (J_z, T_z), (T_z, T_z), (D_z, D_z)$ are also enlarged. In Figs. 5(d) and 5(e), we show orbital-off-diagonal component given by $\Lambda_{1211}^{c,QQ'}$. It takes the largest value for $(Q, Q') = (T_x, D_x)$. Its value for $(Q, Q') = (T_z, D_z), (D_z, D_z), (T_x, T_x), (J_z, D_z)$ are also enlarged.

In summary, in heavy-fermion systems, multiple multipole fluctuations lead to the strong enhancement of U -VC, Λ^c . In Figs. 4(b) and 4(c), both orbital-diagonal and off-diagonal components of Λ^c are enlarged. In Figs. 5(b)–5(e), many pairs of multipole fluctuations (Q, Q') contribute to the enhancement of Λ^c . These facts lead to above-mentioned differences (i) and (ii), which are not seen in $3d$ -electron system. Thus we conclude that the U -VC in f -electron system plays more significant roles due to the strong SOI compared to $3d$ -electron systems.

VII. SUPERCONDUCTIVITY

Now, we discuss obtained superconducting states by solving the gap equation in Eq. (23). The pairing interaction is given by Eqs. (27)–(29). We solve the gap equation in the presence of both u and g , by the following replacement,

$$u \hat{U}^{0;c} \rightarrow u \hat{U}^{0;c} + 2g \hat{W} \quad (42)$$

in $\hat{I}^c(k - k')$ in the pairing interaction (28). For finite g , $\hat{I}^c(\propto \hat{\chi}^c)$ develops as large as \hat{I}^s and $\hat{I}^{s\perp}$. We put $g = 0$ for $\hat{\Lambda}^{ch}$

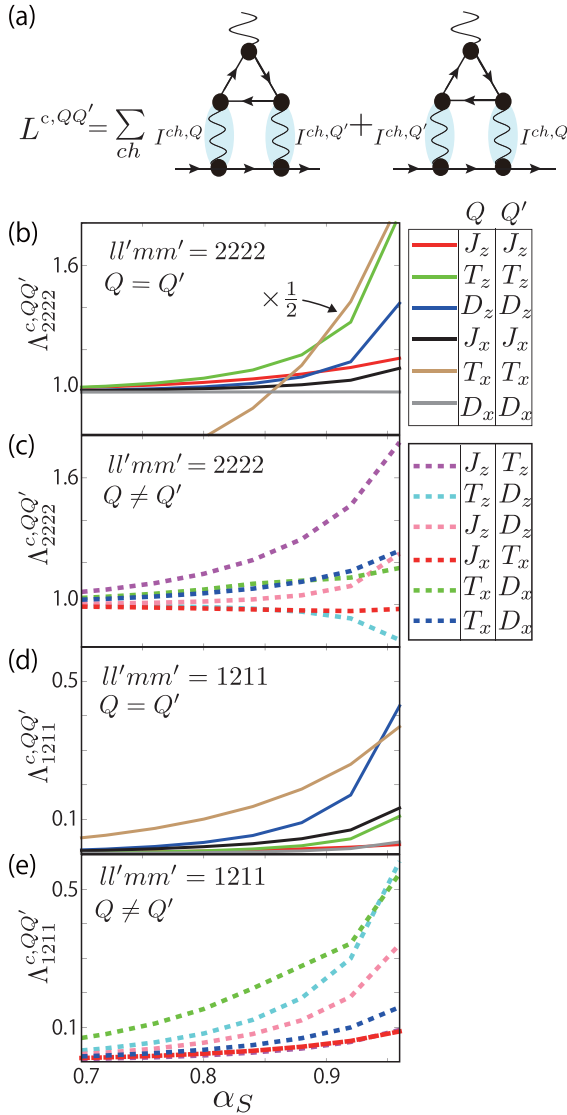


FIG. 5. (a) Multipole-decomposed U -VC given by $\Lambda^{c,QQ'}$. Q and Q' are magnetic multipole operators. Obtained $\hat{\Lambda}_{2222}^{c,QQ'}$ for (b) $Q = Q'$ and (c) $Q \neq Q'$, and $\hat{\Lambda}_{1211}^{c,QQ'}$ for (d) $Q = Q'$ and (e) $Q \neq Q'$. Many pairs of multipole fluctuations (Q, Q') contribute to the enhancement of U -VC.

approximately since the contribution from $\hat{\chi}^c$ remains small even for $g > 0$ [35].

Figures 6(a)–6(b) are obtained phase diagrams, which show the largest eigenvalue and its symmetry of the gap function. In the presence of U -VC, fully gapped s -wave state without any sign reversal emerges when $\alpha_S \lesssim 1$ and $\alpha_C \lesssim 1$ as shown in Fig. 6(a). The region of s -wave phase gets wider as the magnetic fluctuations develop. These results originate from the fact that the charge-channel attractive interaction $-\frac{1}{2}\hat{V}^c$ are strongly enhanced by the charge-channel U -VC, which is enlarged due to the magnetic (odd-rank) multipole fluctuations when $\alpha_S \lesssim 1$. In fact, $-\frac{1}{2}\hat{V}^c$ is expressed as $-\frac{1}{2}\hat{V}^c \propto -\frac{1}{2}|\hat{\Lambda}^c|^2\{(u-2g)^2\chi^c - (u-2g)\}$, which takes large negative (=attractive) value when $\alpha_C \lesssim 1$ [35]. In addition, we find that quite small g is enough for realizing the

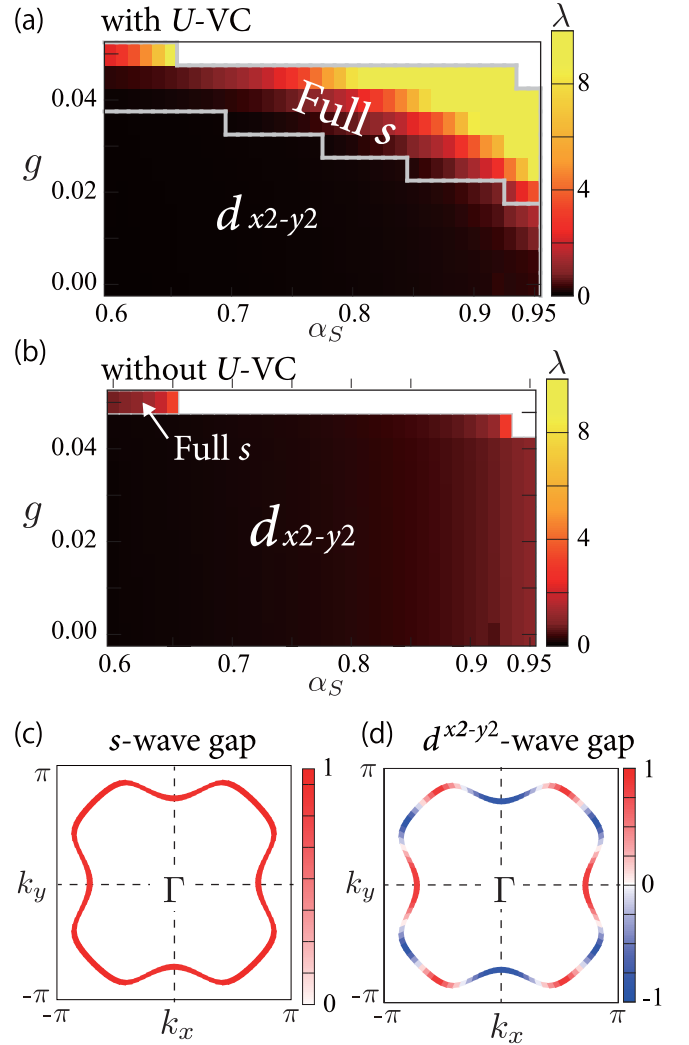


FIG. 6. (a) Phase diagram in the presence of U -VC. The s -wave state emerges due to the significant contribution from U -VC. The white region corresponds to $\alpha_C > 1$. (b) Phase diagram in the absence of U -VC. Anisotropic $d_{x^2-y^2}$ -wave state appears in wide parameter region. The gap function on Fermi surface for (c) s -wave and (d) $d_{x^2-y^2}$ -wave.

s -wave superconductivity. For instance, s -wave state emerges even at $g = 0.025$. This is much smaller than Coulomb interaction $u = 0.31$.

In contrast, the s -wave region in Fig. 6(a) is drastically reduced if we neglect U -VC ($\hat{\Lambda}^{ch} = \hat{1}$) as shown in Fig. 6(b). In this case, $d_{x^2-y^2}$ -wave state appears in wide parameter region. Furthermore, the eigenvalue λ for $d_{x^2-y^2}$ -wave state in Fig. 6(b) is much smaller than that for s -wave state in Fig. 6(a), so T_c of $d_{x^2-y^2}$ -wave state should be very low if realized. Therefore we clearly confirmed that U -VC is important for realizing the s -wave superconductivity. Obtained gap functions on Fermi surface for s - and $d_{x^2-y^2}$ -wave states are expressed in Figs. 6(c) and 6(d), respectively. The obtained s -wave gap function is almost isotropic while the $d_{x^2-y^2}$ -wave gap function has accidental nodes in addition to the symmetry nodes.

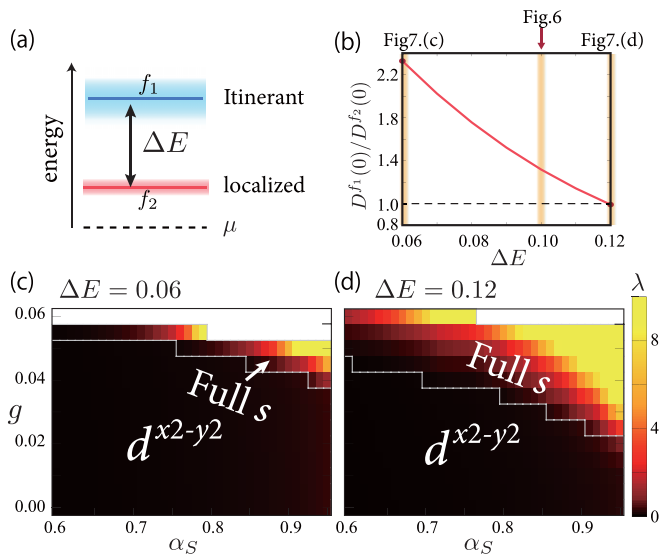


FIG. 7. (a) The energy level of the f -orbital states in the present model. (b) ΔE dependence of the ratio of the DoS $D^{f_1}(0)/D^{f_2}(0)$. The ratio goes to unity at $\Delta E \simeq 0.12$. Obtained phase diagram at (c) $\Delta E = 0.06$ and (d) 0.12 .

In conclusion, once the small electron-phonon interaction exist, fully gapped s -wave superconducting state can appear in f -electron system near the magnetic QCP. This counter-intuitive result is given by the large U -VC caused by multiple (higher-rank) multipole fluctuations. We comment that the obtained large eigenvalues λ in Fig. 6 are overestimated since the self-energy effects (such as the mass renormalization and the quasiparticle damping) are dropped in the gap equation.

Finally, we show that multiorbital nature is a necessary condition for realizing the s -wave superconductivity. In the present model, f orbitals $|f_1\rangle$ and $|f_2\rangle$ have different itinerancy: $|f_1\rangle$ is relatively itinerant and $|f_2\rangle$ is relatively localized. We also introduce the CEF splitting ΔE between $|f_1\rangle$ and $|f_2\rangle$: $E_1 = E_2 + \Delta E$ as shown in Fig. 7(a). In this model, the ratio between the f -orbital DoS at the Fermi level, $D^{f_1}(0)/D^{f_2}(0)$, is much larger than unity at $\Delta E = 0$, and the ratio decreases with ΔE as shown in Fig. 7(b). The ratio reaches unity at $\Delta E \simeq 0.12$. In Figs. 7(c) and 7(d), we show the obtained phase diagram at $\Delta E = 0.06$ and $\Delta E = 0.12$, respectively. The region of s -wave state at $\Delta E = 0.12$ is much wider than that at $\Delta E = 0.06$, which means that s -wave state is favored as ΔE increases. As a result, the condition $D^{f_1}(0) \approx D^{f_2}(0)$ is significant for realizing the s -wave superconducting state. In other words, the multiorbital nature on Fermi surface is important for realizing s -wave states. Therefore the s -wave state emerges in the presence of finite CEF splitting of f levels when the s - f hybridization has strong orbital dependence. This situation is expected to be realized in CeCu_2Si_2 at $P = 0$ [25].

VIII. SUMMARY

In this paper, we proposed a mechanism of s -wave superconductivity in multiorbital heavy-fermion systems based on the recently developed beyond Migdal formalism. In the present two-orbital PAM, various odd-rank multipole

fluctuations strongly develop simultaneously, due to the combination of strong SOI and Coulomb interaction as shown in Fig. 2(b). We verified that the result in Fig. 2(b) is qualitatively same as those for $\Delta E = 0 \sim 0.2$. These developed fluctuations give significant U -VCs, by which the model Coulomb interaction is strongly modified. Especially, the coupling constant between electron and charged-boson ($=u\hat{U}^{0,c} + 2g\hat{W}$) is prominently magnified by the U -VC as shown in Figs. 4 and 5. For this reason, even-rank multipole fluctuations give large attractive interaction when the system is close to the magnetic QCP. We revealed that s -wave superconductivity is strongly enhanced near the magnetic criticality in multiorbital heavy-fermion systems, once moderate phonon-induced multipole fluctuations exist as shown in Fig. 6. Note that the depairing effect of Coulomb interaction is reduced by the multiorbital screening effect [35]. The present mechanism may be responsible for the fully gapped s -wave superconducting state realized in CeCu_2Si_2 .

The main results of the present study on the two-orbital periodic Anderson model with strong SOI are summarized as follows: near the magnetic QCP, we find that (i) several (higher-rank) multipole fluctuations strongly develop simultaneously, whereas rank-1 orbital-diagonal spin susceptibility solely develops in $3d$ -electron systems. (ii) Multiple multipole fluctuations give large U -VC cooperatively, leading to the violation of Migdal theorem. (iii) Thanks to U -VC, electric-multipole fluctuation mediated s -wave superconductivity is realized when $D^{f_1}(0) \approx D^{f_2}(0)$, which is a necessary condition for realizing moderate quadrupole or hexadecapole fluctuations.

In this study, we introduced a phenomenological interaction term in Eq. (11) in order to realize the moderate A_1^+ -channel multipole fluctuations. This term can originate from moderate electron-phonon interaction, as we discussed in the main text. In fact, strong coupling between f electrons and phonons via the s - f hybridization and f -orbital level is expected in heavy-fermion systems, as discussed in Refs. [51–53]. For example, large Gruneisen parameter in heavy-fermion systems ($\eta \equiv -d\log T_K/d\log \Omega \sim 30 - 80$) indicates the significance of electron-phonon interaction [51]. The phonon-mediated s -wave superconductivity in heavy-fermion systems discussed in Refs. [51–53] becomes a realistic scenario by considering the significant role of U -VC revealed in the present study. Another promising microscopic origin of Eq. (11) is the AL-type VCs for the susceptibility. In fact, in $3d$ -electron systems without SOI, the AL-type VCs causes large orbital fluctuations [29]. Recently, the present authors found that the AL-type VCs give large even-rank multipole fluctuations in heavy-fermion systems with strong SOI, which we will discuss in future publication [45].

There are many important future issues. For example, it is interesting to apply the present theory to more realistic three-dimensional model for CeCu_2Si_2 . Also, study of self-energy correction, which gives strong mass-enhancement whereas neglected in the present study, is an important future issue. In addition, the present theory may be applicable for spin-triplet superconductor UPt_3 . In fact, we analyzed the multiorbital Hubbard model for Sr_2RuO_4 , and found that the triplet state is realized under the coexistence of spin and orbital fluctuations [54,55].

ACKNOWLEDGMENTS

We are grateful to Y. Matsuda, T. Shibauchi, Y. Kasahara, S. Kittaka, H. Ikeda, S. Onari, and Y. Yamakawa for useful discussions. This study has been supported by KAKENHI Grants No. 18J12852 and No. 18H01175 from the Japan Society for the Promotion of Science (JSPS).

APPENDIX A: s - f HYBRIDIZATION

Here, we derive the expression of s - f hybridization given in Eq. (4). In the LS basis, the wave functions of f electrons in Eq. (2) are given by

$$|f_1 \uparrow\rangle = a \left\{ \sqrt{\frac{6}{7}} | -3, \uparrow\rangle - \sqrt{\frac{1}{7}} | -2, \downarrow\rangle \right\} + b \left\{ \sqrt{\frac{2}{7}} | 1, \uparrow\rangle - \sqrt{\frac{5}{7}} | 2, \downarrow\rangle \right\}, \quad (\text{A1})$$

$$|f_1 \downarrow\rangle = a \left\{ \sqrt{\frac{1}{7}} | 2, \uparrow\rangle - \sqrt{\frac{6}{7}} | 3, \downarrow\rangle \right\} + b \left\{ \sqrt{\frac{5}{7}} | -2, \uparrow\rangle - \sqrt{\frac{2}{7}} | -1, \downarrow\rangle \right\}, \quad (\text{A2})$$

$$|f_2 \uparrow\rangle = -a \left\{ \sqrt{\frac{2}{7}} | 1, \uparrow\rangle - \sqrt{\frac{5}{7}} | 2, \downarrow\rangle \right\} + b \left\{ \sqrt{\frac{6}{7}} | -3, \uparrow\rangle - \sqrt{\frac{1}{7}} | -2, \downarrow\rangle \right\}, \quad (\text{A3})$$

$$|f_2 \downarrow\rangle = -a \left\{ \sqrt{\frac{5}{7}} | -2, \uparrow\rangle - \sqrt{\frac{2}{7}} | -1, \downarrow\rangle \right\} + b \left\{ \sqrt{\frac{1}{7}} | 2, \uparrow\rangle - \sqrt{\frac{6}{7}} | 3, \downarrow\rangle \right\}, \quad (\text{A4})$$

where \uparrow (\downarrow) is the real spin. Note that the wave functions for $L_z = \pm 2$ are proportional to z as follows:

$$\langle \vec{r} | \pm 2, \sigma \rangle \propto z.$$

Now, we consider the hybridization between f electrons in Eqs. (A1)–(A4) and s electron. In 2D system, the hybridization between s orbitals at \vec{R}_i site and $|\pm 2, \sigma\rangle$ at \vec{R}_j site goes to zero, that is, $\langle s, \sigma, \vec{R}_i | \pm 2, \sigma, \vec{R}_j \rangle = 0$. Then, we obtain

$$\langle s \uparrow | f_1 \uparrow \rangle = \sqrt{\frac{6}{7}} \langle s \uparrow | -3, \uparrow \rangle, \quad (\text{A5})$$

$$\langle s \downarrow | f_1 \downarrow \rangle = -\sqrt{\frac{6}{7}} \langle s \downarrow | 3, \downarrow \rangle, \quad (\text{A6})$$

$$\langle s \uparrow | f_2 \uparrow \rangle = -\sqrt{\frac{2}{7}} \langle s \uparrow | 1, \uparrow \rangle, \quad (\text{A7})$$

$$\langle s \downarrow | f_2 \downarrow \rangle = \sqrt{\frac{2}{7}} \langle s \downarrow | -1, \downarrow \rangle, \quad (\text{A8})$$

where $a = 1$ and $b = 0$. Therefore we obtain the relation $\langle s \uparrow | f_1 \downarrow \rangle = \langle s \downarrow | f_1 \uparrow \rangle = 0$. As a result, we confirm that

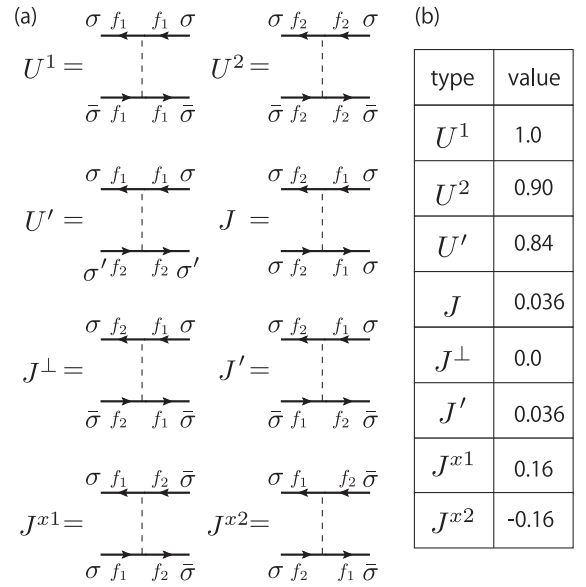


FIG. 8. (a) Definition of multiorbital Coulomb interaction in the pseudospin representation; U^1 , U^2 , J , J^\perp , J' , J^{x1} , and J^{x2} . (b) Obtained value for the Coulomb interaction when $a = 1$ and $(F_0, F_2, F_4, F_6) = (5.3, 9.09, 6.927, 4.756)$ in unit eV. These values are normalized as $U^1 = 1.0$. (Before the normalization, $U^1 = 6.1$ eV.)

the pseudospin is conserved in the s - f hybridization in the present two-orbital model. Therefore we can use the pseudospin channel (s, s^\perp, c), in the present study, which is a great merit for performing detailed analysis.

APPENDIX B: COULOMB INTERACTION

Here, we explain about the Coulomb interaction in Table I in more detail. The Coulomb interaction is obtained by the following steps. First, we calculate the L_z -basis-Coulomb interaction $\bar{U}_{l_z, l'_z, l''_z, l'''_z}$ by using Eq. (6). The obtained Coulomb interaction is written by using the Slater integral parameters (F_0, F_2, F_4, F_6). Note that $\bar{U}_{l_z, l'_z, l''_z, l'''_z} = 0$ for $l_z + l'_z \neq l''_z + l'''_z$. Next, we transfer it from the L_z -basis into the $L = (l, \sigma)$ basis, which is given by the unitary transformation from the right-hand to the left-hand parts in Eqs. (A1)–(A4). The obtained Coulomb interaction satisfies the axial rotational symmetry expressed as Eq. (7) after antisymmetrization. In the case of $a = 1$ and $b = 0$, the obtained Coulomb interaction is written by using the U^1 , U^2 , J , J^\perp , J' , J^{x1} , and J^{x2} . The definition of each element is given in Fig. 8(a), and the obtained values are shown in Fig. 8(b). Although the other elements not listed in Fig. 8 (e.g., $U_{11;12}^{0;ch}$) are zero at $a = 1$, they become finite for $a \lesssim 1$. Note that, in 3d-electron systems without SOI, the relations $J = J^\perp$ and $J^{x1} = J^{x2} = 0$ are satisfied.

Finally, Table I is obtained by introducing the antisymmetrization of the Coulomb interaction. The Table I becomes equal to the table of Coulomb interaction in 3d-electron systems [35] if we put $J = J^\perp$ and $J^{x1} = J^{x2} = 0$ in Table I. We stress that the pseudospin is conserved even for $a \neq 1$.

APPENDIX C: MULTIPOLE OPERATOR

Here, we explain about the multipole operators in Table II. We numerically obtain each operators by using 4×4 tensor $J_q^{(k)}$ in Eq. (10). As a result, electric (even-rank) multipole operators in D_{4h} symmetry are expressed as

$$\begin{aligned}
 A_1^+ & \begin{cases} \hat{I} = \hat{\sigma}^0 \hat{\tau}^0 \\ \hat{O}_{20} = \hat{\sigma}^0 (2.00 \hat{\tau}^0 + 3.00 \hat{\tau}^z) \\ \hat{H}_0 = \hat{\sigma}^0 (-5.73 \hat{\tau}^0 + 11.5 \hat{\tau}^z - 12.8 \hat{\tau}^x) \end{cases}, \\
 A_2^+ & \{ \hat{H}^z = -19.8 \hat{\sigma}^z \hat{\tau}^y, \\
 E^+ & \begin{cases} \hat{O}_{yz} = -3.87 \hat{\sigma}^x \hat{\tau}^y \\ \hat{O}_{zx} = +3.87 \hat{\sigma}^y \hat{\tau}^y \end{cases}.
 \end{aligned} \tag{C1}$$

Magnetic (odd-rank) multipole operators are given by

$$\begin{aligned}
 A_1^- & \{ \hat{D}_4 = +29.8i \hat{\sigma}^0 \hat{\tau}^y, \\
 A_2^- & \begin{cases} \hat{J}^z = \hat{\sigma}^z (0.50 \hat{\tau}^0 + 2.00 \hat{\tau}^z) \\ \hat{T}^z = \hat{\sigma}^z (9.00 \hat{\tau}^0 - 1.50 \hat{\tau}^z), \\ \hat{D}^z = -29.8 \hat{\sigma}^z \hat{\tau}^x \end{cases}, \\
 E^- & \begin{cases} \hat{J}^x = -1.12 \hat{\sigma}^x \hat{\tau}^x \\ \hat{J}^y = -1.12 \hat{\sigma}^y \hat{\tau}^x \\ \hat{T}^x = \hat{\sigma}^x (3.75 \hat{\tau}^0 - 3.75 \hat{\tau}^z + 5.03 \hat{\tau}^x) \\ \hat{T}^y = \hat{\sigma}^y (3.75 \hat{\tau}^0 - 3.75 \hat{\tau}^z + 5.03 \hat{\tau}^x) \\ \hat{D}^x = \hat{\sigma}^x (23.0 \hat{\tau}^0 - 6.56 \hat{\tau}^z - 3.14 \hat{\tau}^x) \\ \hat{D}^y = \hat{\sigma}^y (23.0 \hat{\tau}^0 - 6.56 \hat{\tau}^z - 3.14 \hat{\tau}^x) \end{cases},
 \end{aligned} \tag{C2}$$

where $\hat{\sigma}^\mu$ and $\hat{\tau}^\mu$ ($\mu = x, y, z$) are Pauli matrices for the pseudospin and orbital basis, respectively. $\hat{\sigma}^0$ and $\hat{\tau}^0$ are identity matrices. We express the obtained 16 matrix expressions in Eqs. (C1) and (C1) as O^Q ($Q = (\Gamma, \phi)$). Note that $\sum_{LL'} O_{LL'}^{(\Gamma, \phi)} O_{LL'}^{(\Gamma', \phi')*} = 0$ for $\Gamma \neq \Gamma'$, whereas $\sum_{LL'} O_{LL'}^{(\Gamma, \phi)} O_{LL'}^{(\Gamma, \phi')*} \neq 0$ A_2^+ (E^+) electric multipole operators belong to pseudospin s ($s \perp$) channel since it is proportional to $\hat{\sigma}^z$ ($\hat{\sigma}^x, \hat{\sigma}^y$). Also, A_1^- magnetic multipole operators belong to the charge channel since it is proportional to $\hat{\sigma}^0$. In summary, some electric (magnetic) multipole operators belong to pseudospin (charge) channels as summarized in Table II. The relation between multipole and pseudospin (charge) channels. We have to take care of this fact in analysis.

APPENDIX D: EFFECTS OF f - f HOPPING

In this section, we discuss the effects of f - f hopping. In the main text, we neglected f - f hopping, and therefore the f_l -orbital weight is quite isotropic on Fermi surface as shown in Fig. 1(e). However, this orbital-isotropy can be broken if we introduce finite f - f hopping. Now, we introduce the orbital-dependent f - f hopping. In this case, f -electron energy E_l have \mathbf{k} dependence. As a result, the f_l -orbital weight comes to have θ dependence on the Fermi surface. The f - f hopping is expressed as

$$\hat{H}_{ff} = \sum_{kl\sigma} E_{k,l} f_{kl\sigma}^\dagger f_{kl\sigma}. \tag{D1}$$

Here, we set $E_{k,1} \equiv E_1 + \delta E_k$ and $E_{k,2} \equiv E_2 - \delta E_k$, where the \mathbf{k} -dependence of δE_k is shown in Fig. 9(a). Technically, to realize the δE_k , we introduce the intraorbital f - f hopping

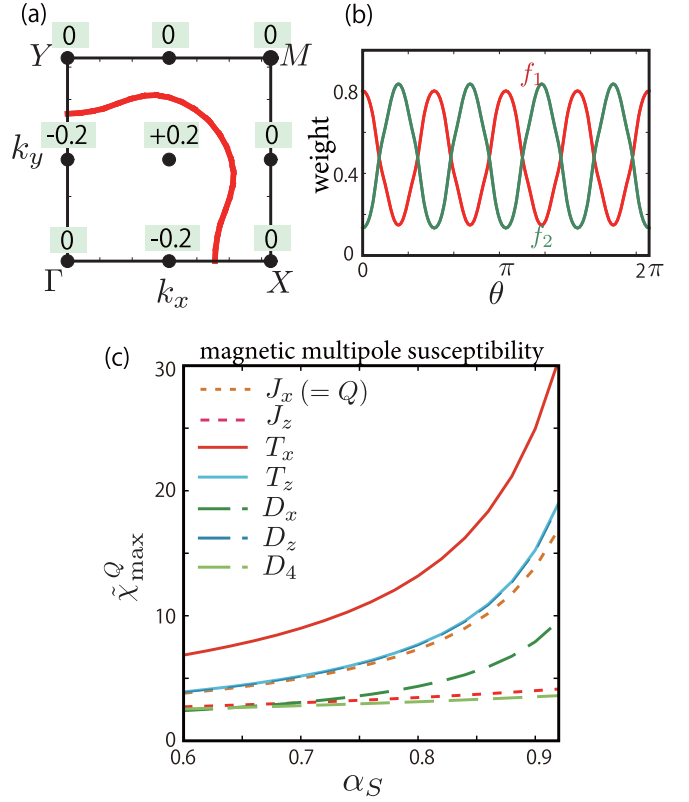


FIG. 9. (a) The Fermi surface with f - f hopping. Each number at \mathbf{k} shows intra-orbital energy shift δE_k . (b) Obtained θ dependence of the f_l -orbital weight on Fermi surface. The red (green) line corresponds to f_1 (f_2) orbital. (c) α_S dependence of magnetic multipole susceptibilities, which are almost equal to those in Fig. 2(b).

up to the fifth nearest-neighbor hopping integrals according to Ref. [36]. In Fig. 9(b), we show the obtained f_l -orbital weight along θ axis on Fermi surface. It shows strong θ dependence irrespective of the fact that $|\delta E_k|$ (~ 0.2) is much smaller than $|t_{sf}|$ ($=0.7$).

One may suspect that higher rank multipole susceptibilities may be suppressed when the f -orbital weight is θ dependent, since the orbital off-diagonal components of $\chi_{ll'mm}^s$ may be suppressed. To answer this question, we perform the RPA analysis. Figure 9(c) shows the obtained magnetic multipole susceptibilities. We find that multiple higher-rank magnetic multipole susceptibilities develop, which is quite similar to our result without f - f hopping in Fig. 2(b). This unexpected results originate from the fact that many body effects away from Fermi energy also contribute to the multipole susceptibility. This result strongly indicates that U - VC is still important even in the presence of small f - f hopping. We study this issue in more detail in the future publication [45].

APPENDIX E: MULTIPOLE EXPANSION

In this section, we explain about the derivation of the coefficient $a^{\Gamma, \phi, \phi'}$ in Eq. (36). First, we solve the characteristic equation for the f -electron susceptibility in the $L = (l, \sigma)$

basis,

$$\sum_{MM'} \chi_{LL'MM'}(q) v_{MM'}^i(q) = \lambda^i(q) v_{LL'}^i(q), \quad (\text{E1})$$

where $\lambda^i(q)$ is i th real eigenvalue ($i = 1 \sim 16$). $v_{LL'}^i(q)$ is a 16-dimensional eigenvector. In the present model, $\chi^{(\Gamma, \phi), (\Gamma', \phi')} = 0$ for $\Gamma \neq \Gamma'$. Thus, for each i , $v_{LL'}^i(q)$ is classified into the corresponding IR (Γ). If we normalize \vec{v}^i as $\sum_{LL'} v_{LL'}^i (v_{LL'}^j)^* = \delta_{i,j}$, the f -electron susceptibility is expressed as

$$\chi_{LL'MM'}(q) = \sum_i v_{LL'}^i(q) \lambda^i(q) v_{MM'}^i(q)^*. \quad (\text{E2})$$

Then, we expand $\vec{v}^i(q)$ for $i \in \Gamma$ on the basis of the multipole matrices $\hat{O}^{(\Gamma, \phi)}$ for $\phi = 1 \sim N_\Gamma$ listed in Eqs. (C1) and (C2) as follows:

$$v_{LL'}^i(q) = \sum_{\phi=1}^{N_\Gamma} b^{i, \phi}(q) O_{LL'}^{(\Gamma, \phi)}, \quad (\text{E3})$$

where the coefficient $b^{i, \phi}(q)$ is uniquely determined. Note that the basis $\{\vec{O}^{(\Gamma, \phi)}\}$ is complete but not orthogonal within the

same Γ . By inserting Eqs. (E3) into (E2), we obtain

$$\chi_{LL'MM'}(q) = \sum_{\Gamma, \phi, \phi'} a^{\Gamma, \phi, \phi'}(q) O_{LL'}^{(\Gamma, \phi)} O_{MM'}^{(\Gamma, \phi')*}, \quad (\text{E4})$$

where

$$a^{\Gamma, \phi, \phi'}(q) = \sum_{i \in \Gamma} b^{i, \phi}(q) \lambda^i(q) b^{i, \phi'}(q)^*. \quad (\text{E5})$$

As a result, the decomposition of $\chi_{LL'MM'}(q)$ in Eq. (36) is obtained. In the same way, the pairing interaction I in Eq. (37) can be decomposed. Using $a^{\Gamma, \phi, \phi'}$, the multipole susceptibility $\chi^{(\Gamma, \phi), (\Gamma', \phi')}$ defined in Eq. (21) is expressed as

$$\chi^{(\Gamma, \phi), (\Gamma', \phi')} = \sum_{\phi'' \phi'''} a^{\Gamma, \phi'', \phi'''} (T_{\phi, \phi''}^\Gamma)^* T_{\phi', \phi'''}^\Gamma, \quad (\text{E6})$$

where

$$T_{\phi, \phi'}^\Gamma = \sum_{MM'} O_{MM'}^{(\Gamma, \phi)} (O_{MM'}^{(\Gamma, \phi')})^*. \quad (\text{E7})$$

-
- [1] T. Moriya and K. Ueda, *Adv. Phys.* **49**, 555 (2000).
- [2] Y. Yanase, T. Jujo, T. Nomura, H. Ikeda, T. Hotta, and K. Yamada, *Phys. Rep.* **387**, 1 (2003).
- [3] H. Kontani, *Rep. Prog. Phys.* **71**, 026501 (2008).
- [4] P. Monthoux, D. Pines, and G. G. Lonzarich, *Nature (London)* **450**, 1177 (2007).
- [5] T. Dahm and L. Tewordt, *Phys. Rev. B* **52**, 1297 (1995).
- [6] P. Monthoux and D. J. Scalapino, *Phys. Rev. Lett.* **72**, 1874 (1994).
- [7] T. Takimoto, T. Hotta, and K. Ueda, *J. Phys.: Condens. Matter* **15**, S2087 (2003).
- [8] R. Shiina, S. Shiba, and T. Peter, *J. Phys. Soc. Jpn.* **66**, 1741 (1997).
- [9] H. Kusunose and Y. Kuramoto, *J. Phys. Soc. Jpn.* **74**, 3139 (2005).
- [10] T. Takimoto, *J. Phys. Soc. Jpn.* **75**, 034714 (2006).
- [11] K. Haule and G. Kotliar, *Nat. Phys.* **5**, 796 (2009).
- [12] R. Okazaki, T. Shibauchi, H. J. Shi, Y. Haga, T. D. Matsuda, E. Yamamoto, Y. Onuki, H. Ikeda, and Y. Matsuda, *Science* **331**, 439 (2011).
- [13] H. Ikeda, M.-T. Suzuki, R. Arita, T. Takimoto, T. Shibauchi, and Y. Matsuda, *Nat. Phys.* **8**, 528 (2012).
- [14] K. Izawa, H. Yamaguchi, Y. Matsuda, H. Shishido, R. Settai, and Y. Onuki, *Phys. Rev. Lett.* **87**, 057002 (2001).
- [15] T. Onimaru, K. T. Matsumoto, Y. F. Inoue, K. Umeo, Y. Saiga, Y. Matsushita, R. Tamura, K. Nishimoto, I. Ishii, T. Suzuki, and T. Takabatake, *J. Phys. Soc. Jpn.* **79**, 033704 (2010).
- [16] A. Sakai and S. Nakatsuji, *J. Phys. Soc. Jpn.* **80**, 063701 (2011).
- [17] F. Steglich, J. Aarts, C. D. Bredl, W. Lieke, D. Meschede, W. Franz, and H. Schafer, *Phys. Rev. Lett.* **43**, 1892 (1979).
- [18] H. Q. Yuan, F. M. Grosche, M. Deppe, C. Geibel, G. Sparn, and F. Steglich, *Science* **302**, 2104 (2003).
- [19] C. Peiderer, *Rev. Mod. Phys.* **81**, 1551 (2009).
- [20] K. Ishida, Y. Kawasaki, K. Tabuchi, K. Kashima, Y. Kitaoka, K. Asayama, C. Geibel, and F. Steglich, *Phys. Rev. Lett.* **82**, 5353 (1999).
- [21] S. Kittaka, Y. Aoki, Y. Shimura, T. Sakakibara, S. Seiro, C. Geibel, F. Steglich, H. Ikeda, and K. Machida, *Phys. Rev. Lett.* **112**, 067002 (2014).
- [22] S. Kittaka, Y. Aoki, Y. Shimura, T. Sakakibara, S. Seiro, C. Geibel, F. Steglich, Y. Tsutsumi, H. Ikeda, and K. Machida, *Phys. Rev. B* **94**, 054514 (2016).
- [23] T. Yamashita, T. Takenaka, Y. Tokiwa, J. A. Wilcox, Y. Mizukami, D. Terazawa, Y. Kasahara, S. Kittaka, T. Sakakibara, M. Konczykowski, S. Seiro, H. S. Jeevan, C. Geibel, C. Putzke, T. Onishi, H. Ikeda, A. Carrington, T. Shibauchi, and Y. Matsuda, *Sci. Adv.* **3**, e1601667 (2017).
- [24] G. Pang, M. Smidman, J. Zhang, L. Jiao, Z. Weng, E. M. Nica, Y. Chen, W. Jiang, Y. Zhang, W. Xie, H. S. Jeevan, H. Lee, P. Gegenwart, F. Steglich, Q. Si, and H. Yuan, *Proc. Natl. Acad. Sci. USA* **115**, 5343 (2018).
- [25] L. V. Pourovskii, P. Hansmann, M. Ferrero, and A. Georges, *Phys. Rev. Lett.* **112**, 106407 (2014). In the present model, we introduce t_{sf} between the nearest Ce sites in the (001) plane. Then, the relation $|V_{k_{f1}\sigma}| \approx 2|V_{k_{f2}\sigma}|$ holds according to Slater-Koster tight-binding methods [42]. In contrast, Pourovskii [25] consider the hybridization between Ce site at $\vec{r} = 0$ and the nearest neighbor Si sites at $(\pm 1/2, \pm 1/2, \pm c)$, and then the relation $|V_{k_{f2}\sigma}| \approx 2|V_{k_{f1}\sigma}|$ holds. In both cases, electric multipole fluctuation mediated superconductivity proposed in this paper is realized when $D^{f_1}(0) \simeq D^{f_2}(0)$ at finite ΔE .
- [26] K. Hattori, *J. Phys. Soc. Jpn.* **79**, 114717 (2010).
- [27] A. T. Holmes, D. Jaccard, and K. Miyake, *Phys. Rev. B* **69**, 024508 (2004).
- [28] H. Ikeda, M.-T. Suzuki, and R. Arita, *Phys. Rev. Lett.* **114**, 147003 (2015).
- [29] S. Onari and H. Kontani, *Phys. Rev. Lett.* **109**, 137001 (2012).

- [30] S. Onari, Y. Yamakawa, and H. Kontani, *Phys. Rev. Lett.* **116**, 227001 (2016).
- [31] Y. Yamakawa, S. Onari, and H. Kontani, *Phys. Rev. X* **6**, 021032 (2016).
- [32] J. R. Schrieffer, *J. Low Temp. Phys.* **99**, 397 (1995).
- [33] M. H. Sharifzadeh Amin and P. C. E. Stamp, *Phys. Rev. Lett.* **77**, 3017 (1996).
- [34] A. B. Migdal, *Zh. Eksp. Teor. Fiz.* **34**, 1438 (1958).
- [35] R. Tazai, Y. Yamakawa, M. Tsuchiizu, and H. Kontani, *J. Phys. Soc. Jpn.* **86**, 073703 (2017).
- [36] Y. Yamakawa and H. Kontani, *Phys. Rev. B* **96**, 144509 (2017).
- [37] A. Georges, G. Kotliar, W. Krauth, and M. J. Rozenberg, *Rev. Mod. Phys.* **68**, 13 (1996).
- [38] G. Kotliar and D. Vollhardt, *Phys. Today* **57**(3), 53 (2004).
- [39] K. Held, *Adv. Phys.* **56**, 829 (2007).
- [40] J. H. Shim, K. Haule, and G. Kotliar, *Science* **318**, 1615 (2007).
- [41] J. Otsuki, *Phys. Rev. Lett.* **115**, 036404 (2015).
- [42] K. Takegahara, Y. Aoki, and A. Yanase, *J. Phys. C* **13**, 583 (1980).
- [43] T. Saso and H. Harima, *J. Phys. Soc. Jpn.* **72**, 1131 (2003).
- [44] A. Amorese, N. Caroca-Canales, S. Seiro, C. Krellner, G. Ghiringhelli, N. B. Brookes, D. V. Vyalikh, C. Geibel, and K. Kummer, *Phys. Rev. B* **97**, 245130 (2018).
- [45] R. Tazai and H. Kontani (unpublished).
- [46] J. C. Slater, *Phys. Rev.* **34**, 1293 (1929).
- [47] M. R. Norman, *Phys. Rev. B* **52**, 1421 (1995).
- [48] T. Inui, Y. Tanabe, and Y. Onodera, *Group Theory and Its Applications in Physics* (Springer, Berlin, 1993).
- [49] H. Kontani and S. Onari, *Phys. Rev. Lett.* **104**, 157001 (2010).
- [50] T. Saito, Y. Yamakawa, S. Onari, and H. Kontani, *Phys. Rev. B* **92**, 134522 (2015).
- [51] H. Razafimandimby, P. Fulde, and J. Keller, *Z. Phys. B* **54**, 111 (1984).
- [52] F. J. Ohkawa, *J. Phys. Soc. Jpn.* **56**, 713 (1987).
- [53] K. Miyake, T. Matsuura, H. Jichu, and Y. Nagaoka, *Prog. Theor. Phys.* **72**, 1063 (1984).
- [54] R. Tazai, Y. Yamakawa, M. Tsuchiizu, and H. Kontani, *Phys. Rev. B* **94**, 115155 (2016).
- [55] M. Tsuchiizu, Y. Yamakawa, S. Onari, Y. Ohno, and H. Kontani, *Phys. Rev. B* **91**, 155103 (2015).